Dynamical Ordering of Non–Birkhoff Orbits and Topological Entropy in the Standard Mapping

Yoshihiro YAMAGUCHI[1] and Kiyotaka TANIKAWA[2]

[1] Teikyo Heisei University, Ichihara, Chiba 290-0193, Japan.

[2] National Astronomical Observatory, Mitaka, Tokyo 181-8588, Japan.

(Received)

Abstract

The standard mapping is an analytical, reversible monotone twist mapping. The appearance ordering, i.e., the so called dynamical ordering, of the symmetric non–Birkhoff periodic orbits (SNBO) in the standard mapping is derived. Essential use is made of the reversibility. After the establishment of various properties of the symmetry axes under the mapping, two theorems on the dynamical ordering are proved. Then the braids for SNBOs are constructed with the aid of techniques developed in the braid group theory. The lower bound of the topological entropy of the system possessing an SNBO is estimated by the eigenvalue of the reduced Burau matrix representation of the braid constructed from the SNBO. Behavior of the topological entropy in the integrable limit is discussed.

1 Introduction

The standard mapping T is defined in cylinder.

$$y_{n+1} = y_n + af(x_n), \quad (1)$$
$$x_{n+1} = x_n + y_{n+1} \ (\mathrm{Mod}\ 2\pi), \quad (2)$$

where a is a positive parameter and $f(x) = \sin x$. There are two fixed points $P = (0, 0)$ and $Q = (\pi, 0)$, where P is a saddle and Q is an elliptic point($0 < a < 4$) or a saddle with reflection($a > 4$). For convenience, we call a point $(2\pi, 0)$ a saddle P'.

As we have repeatedly exploited its property in various occasions,[1,2,14,20,22,23] the standard mapping belongs to a class of systems possessing reversibility(see §2.3). All orbits are classified either into symmetric or non-symmetric ones. The standard mapping belongs to a class of systems which are called monotone twist. All orbits are classified either into monotone or non-monotone ones(§2.2). Symmetric monotone periodic orbits exist down to the integrable limit. In a sense, these objects are not interesting. In order to study the chaotic behavior of the system or how the system becomes more chaotic with parameter, it seems necessary to study other types of periodic orbits. In the standard mapping, symmetric non-monotone periodic orbits are quite suitable for this purpose. There exist non-symmetric periodic orbits bifurcated from symmetric ones.[22]

The appearance order of periodic orbits is called the *dynamical ordering*. The most famous ordering has been proved by Sharkovskii[3] in one–dimensional mappings. Extensions to two–dimensional mappings and to systems described by ordinary differential equations have been carried out by many authors.[4]–[10] In the preceding papers,[1),2)] we studied the dynamical ordering of the symmetric non–Birkhoff orbits in the standard mapping and its family mappings, and in the forced oscillator. In this paper, we extend the dynamical ordering derived in these papers, construct braids for periodic orbits in the dynamical ordering, and estimate the topological entropy of the standard mapping at parameter values for which there are periodic orbits whose braid types are determined. The appearance of non–Birkhoff orbits is related to the non–integrability of systems,[1),2)] and to the breakup of KAM(Kolmogorov–Arnold–Moser) invariant curves.[11),12)]

In §2, we provide several useful concepts and notation used in the following sections. In §3, the properties needed in the proof of theorems are proved. The theorems on the dynamical orderings are proved in §4. The braid for non–Birkhoff orbit listed in the dynamical ordering is constructed in §5 and the topological entropy is estimated in §6. In the final section, we point out several problems to be solved.

2 Preliminaries

2.1 Notation

We have defined the mapping in cylinder. In sections 3 an 4, we almost always work in universal cover $\mathbf{R}^2$ and use the lift mapping. We move from cylinder to universal cover

and vice versa when we construct braids of the non-Birkhoff periodic orbits in section 5. We lift the mapping T to universal cover in such a way that the fixed points of T are also fixed under the lift. Then the lift is uniquely determined. To avoid the notational complexity, we use the same notation T for the lift mapping and coordinates (x, y) for universal cover. We will make a note if there may be a possibility of confusion.

The orbit of a point $z \in \mathbf{R}^2$ is denoted $o(T, z) = \{\ldots, T^{-1}z, z, Tz, \ldots\}$. Following Boyland and Hall,[11] we define the extended orbit of a point $z \in \mathbf{R}^2$ by

$$eo(T, z) = \{T^k z + (2\pi l, 0) : k, l \in \mathbf{Z}\}. \tag{3}$$

We usually abbreviate $o(T, z)$ and $eo(T, z)$ as $o(z)$ and $eo(z)$. Let $\pi_1(z)$(resp. $\pi_2(z)$) be projection to the x-coordinate (resp. y-coordinate) of z. The rotation number ν of an orbit of $z \in \mathbf{R}^2$ is defined as

$$\nu = \limsup_{n\to\infty} \frac{\pi_1(T^n z) - \pi_1(z)}{n}. \tag{4}$$

2.2 Birkhoff and Non-Birkhoff periodic orbits

A point $z \in \mathbf{R}^2$ is called a p/q–periodic point for the standard mapping $T : \mathbf{R}^2 \to \mathbf{R}^2$ if

$$T^q z - (2\pi p, 0) = z.$$

A p/q-periodic point $z \in \mathbf{R}^2$ is called Birkhoff by Hall[15] if for any $r, s \in eo(z)$

$$\pi_1(r) < \pi_1(s) \;\Rightarrow\; \pi_1(Tr) < \pi_1(Ts). \tag{5}$$

Otherwise, the point is said to be non–Birkhoff. A Birkhoff(resp. non-Birkhoff) periodic point is abbreviated as a BP(resp. NBP). Corresponding orbits are denoted as a BO and an NBO.

We give a little bit more precise definition for non-Birkhoff periodic points or orbits. If we lift a p/q-periodic orbit in cylinder to universal cover, there are p different orbits corresponding to the original one. In fact, a p/q-periodic orbit in cylinder has q points in one period. In universal cover, the orbit cover p copies of cylinder in one period. In these copies, there are $q \times p$ points. Therefore, we need p different p/q-periodic orbits. Taking this into account, let us define two types of non-Birkhoff periodic points(NBP).

Definition. Suppose a p/q-periodic point $z \in \mathbf{R}^2$ is given.
(1) If for some $r, s \in eo(z)$ with $r \in o(s)$,

$$\pi_1(r) < \pi_1(s) \;\Rightarrow\; \pi_1(Tr) \geq \pi_1(Ts), \tag{6}$$

then, point z is called a non-Birkhoff periodic point of Type I.
(2) If for any $r, s \in eo(z)$ with $r \in o(s)$,

$$\pi_1(r) < \pi_1(s) \;\Rightarrow\; \pi_1(Tr) < \pi_1(Ts) \tag{7}$$

and if for some $r', s' \in eo(z)$ with $r' \notin o(s')$,

$$\pi_1(r') < \pi_1(s') \Rightarrow \pi_1(Tr') \geq \pi_1(Ts'), \tag{8}$$

then, point z is called a non-Birkhoff periodic point of Type II.

Remarks.
1) Obviously, if a $1/q$-periodic orbit is non-Birkhoff, it is always of Type I. Both Types I and II are possible for p/q–NBOs ($p \geq 2, q \geq 2$).
2) A point $r \in eo(z)$ satisfying

$$\pi_1(T^{-1}r) < \pi_1(r), \pi_1(r) \geq \pi_1(Tr), \text{ or} \tag{9}$$
$$\pi_1(T^{-1}r) > \pi_1(r), \pi_1(r) \leq \pi_1(Tr), \tag{10}$$

is called a turning-back point or simply a turning point. There is an even number of turning-back points in universal cover in an NBO of Type I. There are no turning-back points in an NBO of Type II. Points monotonically proceed to the same direction in the x coordinate under the mapping.

In this paper, we restrict our attention to the first type. An example of NBOs of the second type has been displayed in Refs. 6) and 8).

2.3 Symmetry axes and symmetric periodic orbits

A mapping is reversible if it is decomposed into a product of two involutions.[16] Since the standard mapping is doubly reversible,[14] there are two forms of the product. Roughly speaking, the first one represents the left–right symmetry, i.e., symmetric points are disposed rather horizontally, and the second one the up–down symmetry, i.e., symmetric points are disposed rather vertically. In this paper, we mainly use the first form. Thus T is expressed as the product of involutions H and G.

$$T = H \circ G, \tag{11}$$
$$G : (x, y) \leftrightarrow (-x, y + af(x)) \text{ (Mod } 2\pi), \tag{12}$$
$$H : (x, y) \leftrightarrow (-x + y, y) \text{ (Mod } 2\pi). \tag{13}$$

where $G^2 = id = H^2$ and $\det \nabla G = \det \nabla H = -1$. The sets of fixed points of G and H are the symmetry axes. In universal cover, the symmetry axes are expressed in the forms

$$S_1^{(m)} : x = 2\pi m, \tag{14}$$
$$S_2^{(m)} : x = 2\pi m + \pi, \tag{15}$$
$$S_3^{(m)} : y = 2(x - 2m\pi), \tag{16}$$
$$S_4^{(m)} : y = 2(x - (2m + 1)\pi) \tag{17}$$

where $m(-\infty < m < \infty)$ is an integer. We denote $S_1 = S_1^0$, $S_2 = S_2^0$, $S_3 = S_3^0$, and $S_4 = S_4^0$. S_1 and S_2 are symmetry axes of G, whereas S_3 and S_4 are symmetry axes of H. In order to specify a branch of symmetry axis with $y > 0$ (resp., $y < 0$), we add a suffix $+(-)$ to the expression of axis.

A periodic orbit which has points in symmetry axes is called symmetric. A p/q–periodic symmetric Birkhoff(resp. non-Birkhoff) orbit is denoted by an p/q–SBO(resp. an p/q–SNBO). A point of an SBO(resp. an SNBO) is denoted by an SBP(resp. an SNBP). Let $\{p_0, p_1, \cdots, p_{q-1}\}$ be a set of points from one period of an p/q–SBO or an p/q–SNBO. We summarize the relation of these points and the symmetry axes in Table I.[12),16)]

Table I. The relation of the symmetry axes and the symmetric periodic orbits.

$p(\geq 0)$	q	p_0	Transit	$p(\geq 0)$	q	p_0	Transit
Odd	$2k$	S_1	$p_k \in S_2$	Odd	$2k+1$	S_1	$p_{k+1} \in S_4$
Odd	$2k$	S_2	$p_k \in S_1$	Odd	$2k+1$	S_2	$p_{k+1} \in S_3$
Odd	$2k$	S_3	$p_k \in S_4$	Odd	$2k+1$	S_3	$p_k \in S_2$
Odd	$2k$	S_4	$p_k \in S_3$	Odd	$2k+1$	S_4	$p_k \in S_1$
Even	$2k$	S_1	$p_k \in S_1$	Even	$2k+1$	S_1	$p_{k+1} \in S_3$
Even	$2k$	S_2	$p_k \in S_2$	Even	$2k+1$	S_2	$p_{k+1} \in S_4$
Even	$2k$	S_3	$p_k \in S_3$	Even	$2k+1$	S_3	$p_k \in S_1$
Even	$2k$	S_4	$p_k \in S_4$	Even	$2k+1$	S_4	$p_k \in S_2$

Here we present an easy way to distinguish SNBPs from SBPs and distinguish two types of SNBPs. Let us suppose that a p/q–periodic point is bifurcated in a symmetry axis. We claim that this is a non-Birkhoff periodic point. Indeed, let us suppose the point is bifurcated in either S_1 or S_2. We already have an p/q–SBP in the axis. This means that the whole p/q–periodic orbits are not in the graph of a Lipschitz function,[4),6)] which implies that new born point is a non-Birkhoff point. Next, let us take a positive rotation number and suppose a point r is bifurcated in either S_{3+} or S_{4+}. Let s be the Birkhoff point in the axis. Assume that r and s satisfy the relation $\pi_1(r) < \pi_1(s)$. One easily confirms that $\pi_1(T^{-1}r) > \pi_1(T^{-1}s)$. This means either r or s is non-Birkhoff. Then r is non-Birkhoff. For a negative rotation number we take points in S_{3-} or S_{4-} and argue in a similar manner.

Thus we have proved

Proposition 2.1. Symmetric periodic points bifurcated in symmetry axes and stay there are SNBPs.

Next let us see, using examples, the geometrical difference of SNBPs of Types I and II. Suppose that $T^2r \in T^2S_{1+}^{(0)} \cap S_{4-}^{(0)}$. Then $r \in S_{1+}$ is an 1/3-SNBP of Type I, since $\pi_1(r) < \pi_1(Tr)$ and $\pi_1(Tr) > \pi(T^2r)$. Suppose that $T^2r \in T^2S_{1+}^{(0)} \cap S_{3+}^{(1)}$ and this point is bifurcated via saddle–node bifurcation. Then $r \in S_{1+}^0$ is an 2/3-SNBP of Type II, since $\pi_2(r), \pi_2(Tr)$, $\pi_2(T^2r)$ are all positive and there are no turning-back points.

2.4 Stable and unstable manifolds

Two saddles P and P' have stable and unstable manifolds. Let W_u^1 be a branch of unstable manifold starting at P toward the right direction and W_s^1 be a branch of stable manifold going toward P' from the left side in universal cover. Let W_u^2 be a branch of unstable manifold starting at P' and W_s^2 be a branch of stable manifold going toward P (see Fig. 1).

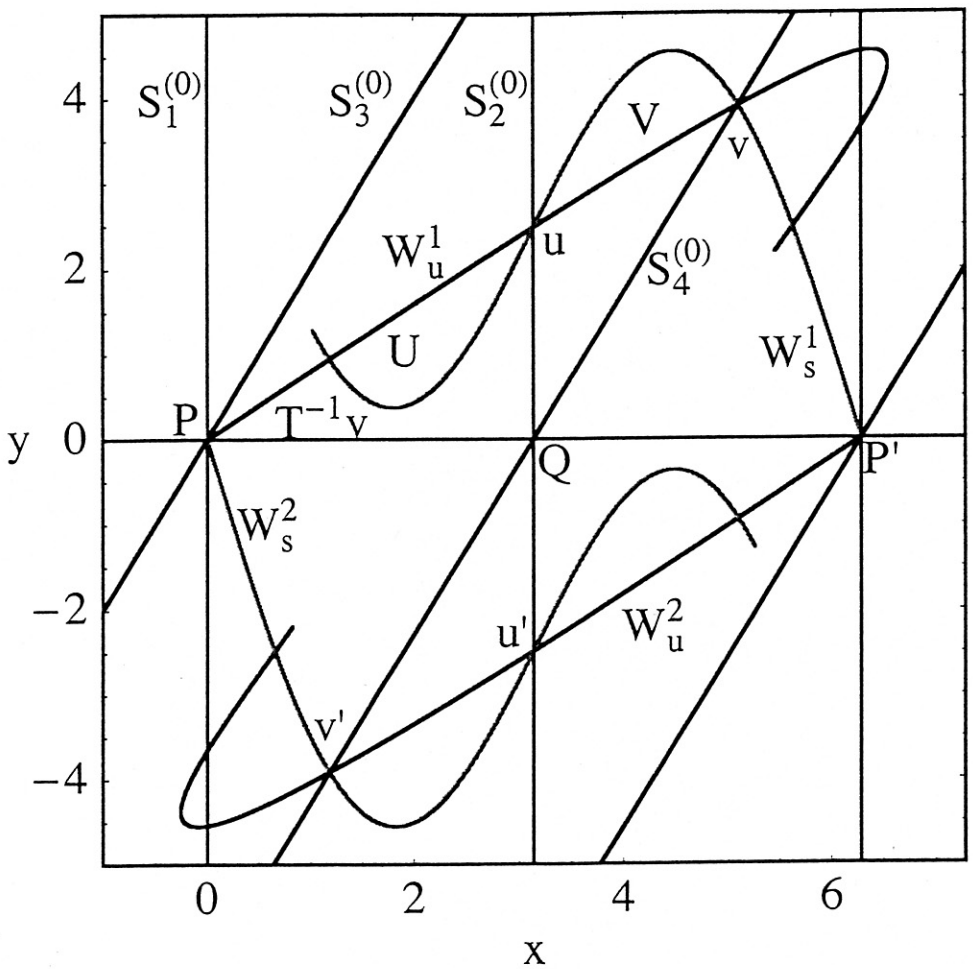

Fig. 1. Structure of stable and unstable manifolds in the standard mapping at $a = 3.2$. The symmetry axes $S_i^{(0)} (i = 1, \cdots, 4)$ are also displayed.

The existence of transverse intersection of W_u^1 and W_s^1 at u has been proved,[18] where u is an intersection point of W_u^1 and $S_{2+}^{(0)}$. The slope of W_s at u is larger than that of W_u. Due to the up–down symmetry, two unstable manifolds W_u^1 and W_u^2 are symmetric with respect to Q. This is the case also for W_s^1 and W_s^2. Hence W_u^2 and W_s^2 intersect transversely at u' where u' is the symmetrical point of u with respect to Q. Due to the

reversibility, the stable and unstable manifolds are related by

$$GW_u^i = W_s^i, \tag{18}$$
$$HW_u^i = W_s^i, \tag{19}$$

with $i = 1, 2$.

Let $r, s \in W_u$ where r is closer to P than s is along W_s. A closed arc of W_u between r and s will be written as $[r, s]_{W_u}$. Open and semi-open arcs are defined similarly. Arcs of other manifolds are defined in a similar manner. Points u and v, and their forward and backward iterates are the primary homoclinic points.[19] Let $\gamma_u = [u, v]_{W_u^1}$ and $\gamma_s = [u, v]_{W_s^1}$. Let V be an open region bounded by γ_u and γ_s and U an open region bounded by $[T^{-1}v, u]_{W_u^1}$ and $[T^{-1}v, u]_{W_s^1}$. These are primary homoclinic lobes. Due to Eq. (18), two lobes U and V are related by

$$U = GV. \tag{20}$$

We define the open intervals in the symmetry axes.

$$I_n^{(-m)} = T^{-n}V \cap S_{1+}^{(-m)} \ (m \geq 0, n \geq 1), \tag{21}$$
$$J_n^{(-m)} = T^{-n}V \cap S_{2+}^{(-m)} \ (m \geq 1, n \geq 1), \tag{22}$$
$$K_n^{(-m)} = T^{-n}V \cap S_{3+}^{(-m)} \ (m \geq 0, n \geq 0), \tag{23}$$
$$L_n^{(-m)} = T^{-n}V \cap S_{4+}^{(-m)} \ (m \geq 1, n \geq 0). \tag{24}$$

These may be empty for a certain range of parameter values. In Fig. 2, several intervals are displayed. We further introduce

$$I^{(-m)} = \cup_{n \geq 1} I_n^{(-m)}, \quad J^{(-m)} = \cup_{n \geq 1} J_n^{(-m)}, \tag{25}$$
$$K^{(-m)} = \cup_{n \geq 0} K_n^{(-m)}, \quad L^{(-m)} = \cup_{n \geq 0} L_n^{(-m)}. \tag{26}$$

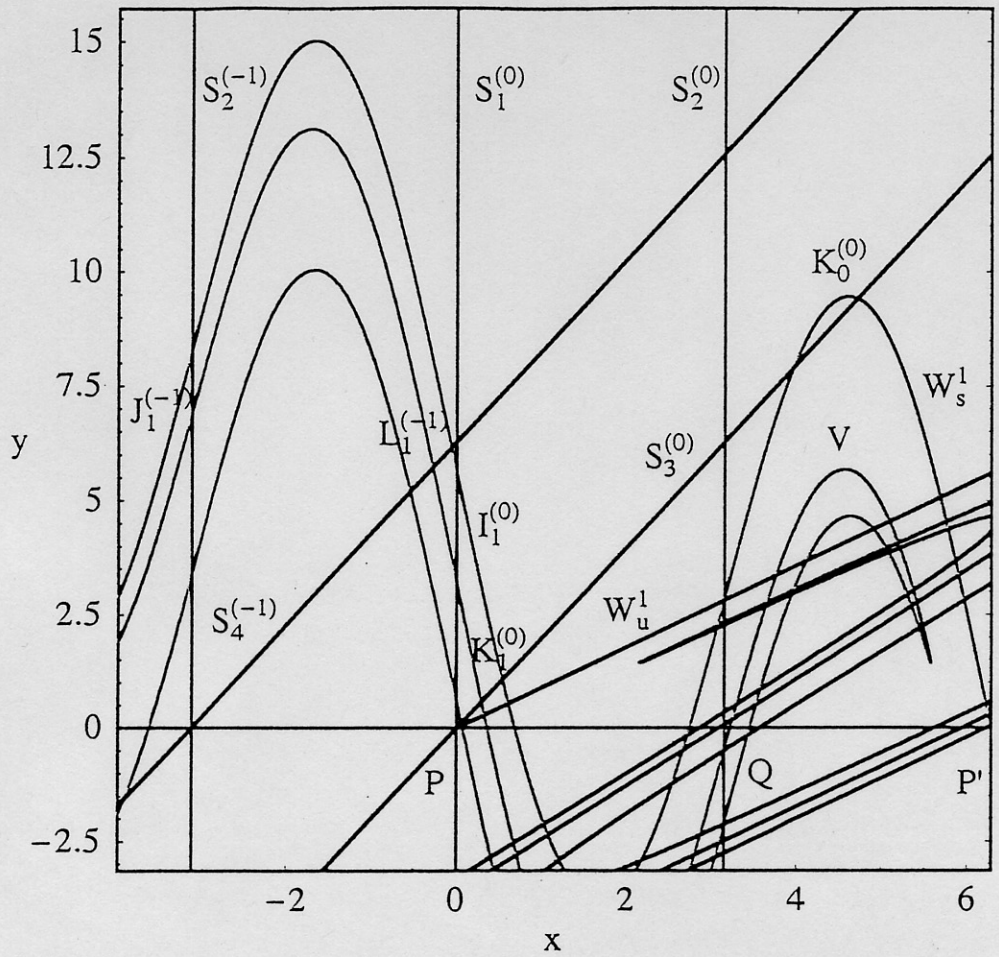

Fig. 2. Intervals $I_1^{(0)}$, $J_1^{(-1)}$, $K_0^{(0)}$, $K_1^{(0)}$ and $L_1^{(-1)}$ are observed at $a = 8$.

We write

$$p/q \in I_n^{(-m)} \tag{27}$$

if an p/q–SNBP exists in $I_n^{(-m)}$. We use the same notation for other intervals. We define the critical parameter values.

[1] $a_c(p/q \in I_n^{(-m)}) = \inf\{a > 0 : p/q \in I_n^{(-m)}\}$.

[2] $a_c(I_n^{(-m)}) = \inf\{a > 0 : I_n^{(-m)} \neq \emptyset\}$.

The critical values for SNBPs in other intervals are similarly defined.

3 Properties

Property 3.1. Let $r \in V$ and $s \in U$. Then we have

$$\pi < \pi_1(r) < 2\pi, \tag{28}$$

$$0 < \pi_1(s) < \pi. \tag{29}$$

Proof. We have $\pi_1(u) = \pi$ and $\pi < \pi_1(v) < 2\pi$. Thus V is located in the region between $x = \pi$ and $x = 2\pi$. The first relation is proved. Equation (20) implies the second one. Q.E.D.

Let D be an open region bounded by $B_1 = [Q, u]_{S_2^{(0)}}$, $B_2 = [u, v]_{W_u^1}$, $B_3 = [v, P']_{W_s^1}$, and $B_4 = [Q, P']$ in the x axis, and let Z be an open region outside D satisfying $y > 0$ and $y < 2(x - \pi)$.

Property 3.2.

$$TD \cap Z = \emptyset. \tag{30}$$

Proof. TB_1 is a line segment of $y = x - \pi$ in D and then $TB_1 \cap Z = \emptyset$. TB_3 is $[Tv, P']_{W_s^1}$. One easily confirms $\pi_2(Ts) < 0$ for any $s \in B_4 \backslash \{Q, P'\}$. So $TB_4 \cap Z = \emptyset$. Since $TB_2 \cap TB_4 = \emptyset$ holds, TV is located in the region surrounded by TB_1, $[Tu, P']_{W_s^2}$, and TB_4. Thus we have $TB_2 \cap Z = \emptyset$. Q.E.D.

Property 3.3. Any periodic point in primary homoclinic lobe V is an NBP of Type I.
Proof. Let $z \in V$ be a p/q–periodic point. The relation $\pi_1(z) - \pi_1(T^{-1}z) = \pi_2(z) > 0$ holds. The orbit of z goes forward from $T^{-1}z$ to z. Thus the existence of turning-back is obvious if $p \leq 0$. So we take $p > 0$. A point of TV is either in D or below the x-axis. A point below the x-axis is a turned-back point. A point of $TV \subset D$ under one more iterate decreases its y-coordinate but never go into Z by Property 3.2. Since z is a periodic point, its finite iterate goes out of D. It necessarily goes below the x-axis. Therefore in any case, the orbit of z has a turning-back point. Q.E.D.

Property 3.4. $I_n^{(-m)}$ consists of a unique component. The same is true for other intervals.
Proof. Let $\gamma_s = [u, v]_{W_s^1}$. The slope of the graph of γ_s strictly decreases as x increases.[20] The largest slope is at u and is greater than 1. So there is a unique point $w \in \gamma_s$ at which the slope is 1. Then $T^{-1}\gamma_s$ has a unique point $T^{-1}w$ at which the slope diverges. This implies that there is only one component in $I_1^{(0)}$ if $I_1^{(0)}$ exists at all.

If $I_2^{(0)}$ has two components, there exist at least three points in the arc $T^{-2}\gamma_s$ at which the slope diverges. Then $T^{-1}\gamma_s$ has at least three points at which the slope is equal to 1, and thus it has at least three points at which the slope diverges. This contradicts the above mentioned property of $T^{-1}\gamma_s$. Repeating this procedure, the statement is proved. Q.E.D.

Property 3.5. The critical values satisfy the following relations.

$$a_c(I_{n+1}^{(-m)}) < a_c(I_n^{(-m)}),\ a_c(J_{n+1}^{(-m)}) < a_c(J_n^{(-m)})\ (m \geq 0, n \geq 1), \tag{31}$$

$$a_c(K_{n+1}^{(-m)}) < a_c(K_n^{(-m)}),\ a_c(L_{n+1}^{(-m)}) < a_c(L_n^{(-m)})\ (m \geq 0, n \geq 0), \tag{32}$$

$$a_c(I_n^{(-m)}) < a_c(I_n^{(-m-1)}),\ a_c(J_n^{(-m)}) < a_c(J_n^{(-m-1)})\ (m \geq 0, n \geq 1), \tag{33}$$

$$a_c(K_n^{(-m)}) < a_c(K_n^{(-m-1)}),\ a_c(L_n^{(-m)}) < a_c(L_n^{(-m-1)})\ (m \geq 0, n \geq 0), \tag{34}$$

$$a_c(J_n^{(-m-1)}) > a_c(L_n^{(-m-1)}) > a_c(I_n^{(-m)}) > a_c(K_n^{(-m)})\ (m \geq 0), \tag{35}$$

$$a_c(K_n^{(-m)}) > a_c(I_{n+1}^{(-m)})\ (m \geq 0), \tag{36}$$

$$a_c(L_n^{(-m)}) > a_c(J_{n+1}^{(-m)})\ (m \geq 0). \tag{37}$$

Proof. Equations (31)–(35) follow from the construction of intervals and the lambda lemma.[21] We shall give a proof of Eq. (36). Let us increase the parameter and suppose $T^{-1}[u, v]_{W_s^1}$ touches $S_{3+}^{(0)}$ for the first time at some a. There exist an interval in $y = x (x \geq 0)$ such that two end points are intersection points of $T^{-1}[u, v]_{W_s^1}$ and $y = x (x \geq 0)$. By definition, the backward image of this interval is $I_2^{(0)}$. Thus we have the relation $a_c(K_1^{(0)}) > a_c(I_2^{(0)})$. Repeating this, Eq. (36) is proved. The proof for Eq. (37) is similar. Q.E.D.

Property 3.6.

$$\lim_{n\to\infty} a_c(R_n^{(-m)}) = 0 \tag{38}$$

where $R = \{I, J\}\ (m \geq 0, n \geq 1)$ and $R = \{K, L\}\ (m \geq 0, n \geq 0)$.

Proof. According to the lambda lemma, the intersection of $W_{u(s)}^1$ and $S_{1+}^{(-m)}$ exists for any small $a > 0$. This implies Eq. (38). Q.E.D.

Property 3.7.

$$\lim_{n\to\infty} T^n R_n^{(-m)} = \gamma_u \tag{39}$$

where R is defined in Property 3.6.

Proof. For simplicity let us only consider the case $R = I$ and $m = 0$. The proof for other R and m is basically the same. Let $\Gamma = [v, Tu]_{W_u^1}$ and let $\Gamma^{(-k)}$ be the set of points of Γ shifted to the left by $2k\pi, k \geq 1$. Obviously $\Gamma^{(-k)}$ is an arc of the unstable manifold emanating from a fixed point at $(-2k\pi, 0)$. For a given $a > 0$, there is a minimum $k_0 \geq 1$ such that $\Gamma^{(-k_0)} \cap S_{1+}^0 = \emptyset$. Let $\hat{\Gamma} = \Gamma^{(-k_0)}$. By the lambda lemma, $T^n\hat{\Gamma}$ has an arc arbitrarily close to $[P, v]_{W_u^1}$ for sufficiently large $n > 0$. $T^n I_n^0$ is sandwiched by $T^n\hat{\Gamma}$ and $[P, v]_{W_u^1}$. Q.E.D.

Property 3.8. If $I_n^{(-m)}$ exists at all, then it contains SNBPs of Type I. The same property holds for other intervals $J_n^{(-m)}$, $K_n^{(-m)}$ and $L_n^{(-m)}$.

Proof. In view of Property 3.3, we need only to show that $I_n^{(-m)}$ contains a periodic point, i.e., $T^k I_n^{(-m)}$ intersects another symmetry axis for some $k > 0$. By the lambda lemma, there exists a positive j_0 such that $T^j\gamma_u \cap S_{2-}^{(0)} \neq \emptyset$ for $j \geq j_0$ and in addition, intersections are transverse. By Property 3.7, $T^n I_n^{(-m)}$ is arbitrarily close to γ_u as a whole for sufficiently large n. Then one confirms that $T^k I_n^{-m} \cap S_{2-}^{(0)} \neq \emptyset$ for $k = n + j$ for sufficiently large $j \geq j_0$. The proofs for other cases are similar and omitted. Q.E.D.

Property 3.8 gives two relations for the critical values.

$$a_c(p/q \in R_n^{(-m)}) > a_c(R_n^{(-m)}), \tag{40}$$

$$\lim_{q\to\infty} a_c(p/q \in R_n^{(-m)}) = a_c(R_n^{(-m)}) \tag{41}$$

where R is defined in Property 3.6.

Property 3.9. The minimum period of SNBPs in $I_n^{(-m)}$ or $J_n^{(-m)}$ is $2n+1$ where $n \geq 1$. The minimum period of SNBPs in $K_n^{(-m)}$ or $L_n^{(-m)}$ is $2n+2$ where $n \geq 0$.

Proof. We know that $T^n I_n^{(-m)} \subset V$. At least one iteration is needed to go from V to U. Due to the symmetry with respect to G, n iterations are needed to go from U to $I_n^{(-m+1)}$, which is $I_n^{(-m)}$ shifted by 2π toward the right direction. Thus the first statement is proved.

We know that $T^n K_n^{(-m)} \subset V$. At least one iteration is needed to go from V to U, and $(n+1)$ iterations are needed to go from U to $K_n^{(-m+1)}$ due to the symmetry with respect to H. The second statement is proved. Q.E.D.

4 Dynamical ordering

There are many types of SNBOs with $2n(n \geq 1)$ turning points if its period is large enough. For example, if the period is five, SNBOs with two and four turning points are possible. In the following, we restrict our attention to p/q–SNBOs $(p \geq 0, q \geq 2)$ with two turning points.

We introduce two symbols $\rightarrow$ ($\downarrow$) and $\leftrightarrow$. Let R, R' be one of I, J, K, or L. If the existence of an p/q–SNBP in $R_n^{(-m)}$ implies the existence of an p'/q'–SNBP in $R_{n'}^{\prime(-m')}$, then we write as

$$\frac{p}{q} \in R_n^{(-m)} \rightarrow \frac{p'}{q'} \in R_{n'}^{\prime(-m')}, \tag{42}$$

If both an p/q–SNBP in $R_n^{(-m)}$ and an p'/q'–SNBP in $R_{n'}^{\prime(-m')}$ appear at the same value of a, then

$$\frac{p}{q} \in R_n^{(-m)} \leftrightarrow \frac{p'}{q'} \in R_{n'}^{\prime(-m')}. \tag{43}$$

4.1 Dynamical ordering for $p/2$– and $p/3$–SNBOs

In the dynamical ordering derived in the next subsection, $p/2$– or $p/3$–SNBOs occupy special positions. We summarize their properties in this section.

Property 3.9 implies that an $p/2$–SNBP appears in $K_0^{(-m)}$ and $L_0^{(-m)}$. A dynamical ordering among them proved in Ref. 22) is reproduced in Table II. For completeness sake, we cite the short proof.

Table II. Dynamical ordering for $p/2$–SNBPs.

$K_0^{(0)}$	$\leftarrow$	$L_0^{(-1)}$	$\leftarrow$	$K_0^{(-1)}$	$\leftarrow$	$L_0^{(-2)}$	$\leftarrow$
						$0/2$	$\leftarrow$
						$\downarrow$	$\nwarrow$
				$0/2$	$\leftarrow$	$1/2$	$\leftarrow$
				$\downarrow$	$\nwarrow$	$\downarrow$	$\nwarrow$
		$0/2$	$\leftarrow$	$1/2$	$\leftarrow$	$2/2$	$\leftarrow$
		$\downarrow$	$\nwarrow$	$\downarrow$	$\nwarrow$	$\downarrow$	$\nwarrow$
$0/2$	$\leftarrow$	$1/2$	$\leftarrow$	$2/2$	$\leftarrow$	$3/2$	$\leftarrow$
$\downarrow$	$\nwarrow$	$\downarrow$	$\nwarrow$	$\downarrow$	$\nwarrow$	$\downarrow$	$\nwarrow$
$1/2$	$\leftarrow$	$2/2$	$\leftarrow$	$3/2$	$\leftarrow$	$4/2$	$\leftarrow$

Proof of Table II. We estimate the critical values $a_c(p/2 \in K_0^{(-m)})$ and $a_c(p/2 \in L_0^{(-m)})$, at which an $p/2$–SNBP appears in the corresponding interval.

$$a_c(p/2 \in K_0^{(-m)}) \approx 2\pi(3 + 4m - p) \quad (n \geq 0, 2m + 1 \geq p \geq 0), \tag{44}$$

$$a_c(p/2 \in L_0^{(-m)}) \approx 2\pi(1 + 4m - p) \quad (n \geq 1, 2m \geq p \geq 0). \tag{45}$$

The fact that the x coordinate of $p/2$–SNBP is approximately equal to $3\pi/2$ is used. Equations (44) and (45) determine the dynamical ordering in Table II. Q.E.D.

We consider $p/3$–SNBPs appearing in $I_0^{(-m)}$ and $J_0^{(-m)}$. The detailed discussion has been done in Ref. 23). We show in Table III the extended ordering including the case with $p = 0$.

Table III. Dynamical ordering for $p/3$–SNBPs.

$I_1^{(0)}$	$\leftarrow$	$J_1^{(-1)}$	$\leftarrow$	$I_1^{(-1)}$	$\leftarrow$	$J_1^{(-2)}$	$\leftarrow$
						$0/3$	$\leftarrow$
						$\downarrow$	
				$0/3$	$\leftarrow$	$1/3$	$\leftarrow$
				$\downarrow$		$\downarrow$	
		$0/3$	$\leftarrow$	$1/3$	$\leftarrow$	$2/3$	$\leftarrow$
		$\downarrow$		$\downarrow$		$\downarrow$	
$0/3$	$\leftarrow$	$1/3$	$\leftarrow$	$2/3$	$\leftarrow$	$3/3$	$\leftarrow$
$\downarrow$		$\downarrow$		$\downarrow$		$\downarrow$	
$1/3$	$\leftarrow$	$2/3$	$\leftarrow$	$3/3$	$\leftarrow$	$4/3$	$\leftarrow$

Proof of Table III We estimate the critical values $a_c(p/3 \in I_1^{(-m)})$ and $a_c(p/3 \in J_1^{(-m)})$, at which an $p/3$–SNBP appears in the corresponding interval.

$$a_c(p/3 \in I_1^{(-m)}) \approx 2(3m - p + 9/4)\pi \quad (i \geq 0, 2m + 1 \geq p \geq 0), \tag{46}$$

$$a_c(p/3 \in J_1^{(-m)}) \approx 2(3m - p + 3/4)\pi \quad (i \geq 1, 2m \geq p \geq 0). \tag{47}$$

The fact that the x coordinate of $p/3$–SNBP is approximately equal to $3\pi/2$ is used. Equations (46) and (47) determine the dynamical ordering in Table III. Q.E.D.

4.2 Two theorems

Theorem 1. The following dynamical ordering for p/q–SNBPs in $I_n^{(-m)}$ and $J_n^{(-m)}$ holds with $0 \leq p \leq (2m + 1)$ for $I_n^{(-m)}$, and $0 \leq p \leq 2m$ for $J_n^{(-m)}$.

$I_0^{(-m)}, J_0^{(-m)}$:	$p/3$	$\rightarrow$	$p/4$	$\rightarrow$	$p/5$	$\rightarrow$	$p/6$	$\rightarrow$
	$\downarrow$		$\downarrow$		$\downarrow$		$\downarrow$	
$I_1^{(-m)}, J_1^{(-m)}$:	$p/5$	$\rightarrow$	$p/6$	$\rightarrow$	$p/7$	$\rightarrow$	$p/8$	$\rightarrow$
	$\downarrow$		$\downarrow$		$\downarrow$		$\downarrow$	
$I_2^{(-m)}, J_2^{(-m)}$:	$p/7$	$\rightarrow$	$p/8$	$\rightarrow$	$p/9$	$\rightarrow$	$p/10$	$\rightarrow$
	$\downarrow$		$\downarrow$		$\downarrow$		$\downarrow$	

Proof. The conditions for p are determined by Eqs (46) and (47). We prove the cases for SNBPs in $I_n^{(-m)}$. The proof for SNBPs in $J_n^{(-m)}$ is similar, and thus is omitted.

(1) Proof of $p/k \in I_n^{(-m)} \to p/(k+1) \in I_n^{(-m)} (k \geq 2n+1)$.

(1-1) Both p and k are odd.

The assumption $p/k \in I_n^{(-m)}$ implies the relation $T^{(k+1)/2} I_n^{(-m)} \cap S_{4-}^{-(m-(p-1)/2)} \neq \emptyset$. Relation $T^{(k+1)/2} I_n^{(-m)} \cap S_{2-}^{-(m-(p-1)/2)} \neq \emptyset$ follows from the relative positions of $S_{2-}^{-(m-(p-1)/2)}$ and $S_{4-}^{-(m-(p-1)/2)}$. In fact, $S_{4-}^{-(m-(p-1)/2)}$ is located to the left side of $S_{2-}^{-(m-(p-1)/2)}$. The intersection points are those of SNBO with $\nu = p/(k+1)$ starting from $I_n^{(-m)}$.

(1-2) p is odd and k is even.

The assumption implies the relation $T^{k/2} I_n^{(-m)} \cap S_{2-}^{-(m-(p-1)/2)} \neq \emptyset$. The intersection points are mapped under T to the left of $S_{4-}^{-(m-(p-1)/2)}$ (see Fig. 3). This implies $T^{(k+2)/2} I_n^{(-m)} \cap S_{4-}^{-(m-(p-1)/2)} \neq \emptyset$.

(1-3) p is even and k is odd.

The proof is similar to (1-1), and thus is omitted.

(1-4) Both p and k are even.

The proof is similar to (1-2), and thus is omitted.

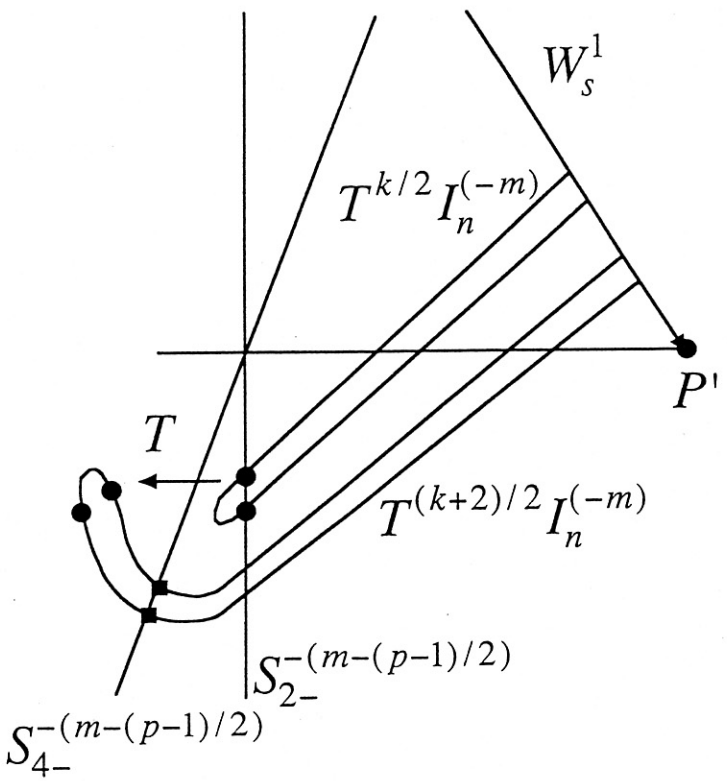

Fig. 3. Disposition of $S_{2-}^{-(m-(p-1)/2)}$ and $S_{4-}^{-(m-(p-1)/2)}$ and that of $T^{k/2} I_n^{(-m)}$ and $T^{(k+2)/2} I_n^{(-m)}$.

(2) Proof of $p/k \in I_n^{(-m)} \to p/(k+2) \in I_{n+1}^{(-m)}$ $(k \geq 2n+1)$.
(2-1) Both p and k are odd.

The assumption $p/k \in I_n^{(-m)}$ implies $T^{(k+1)/2} I_n^{(-m)} \cap S_{4-}^{-(m-(p-1)/2)} \neq \emptyset$. The relative positions of $T^{(k+1)/2} I_n^{(-m)}$ and $T^{(k+3)/2} I_{n+1}^{(-m)}$ are displayed in Fig. 4. $T^{(k+3)/2} I_{n+1}^{(-m)}$ is located outside the closed area bounded by $T^{(k+1)/2} I_n^{(-m)}$ and an arc of W_s^1. We express this configuration $T^{(k+3)/2} I_{n+1}^{(-m)} \dashv T^{(k+1)/2} I_n^{(-m)}$. This implies $T^{(k+3)/2} I_{n+1}^{(-m)} \cap S_{4-}^{-(m-(p-1)/2)} \neq \emptyset$. The intersection points are those of $p/(k+2)$–SNBOs starting in $I_{n+1}^{(-m)}$.

For the other cases, the proofs are similar to (2-1), and thus are omitted. Q.E.D.

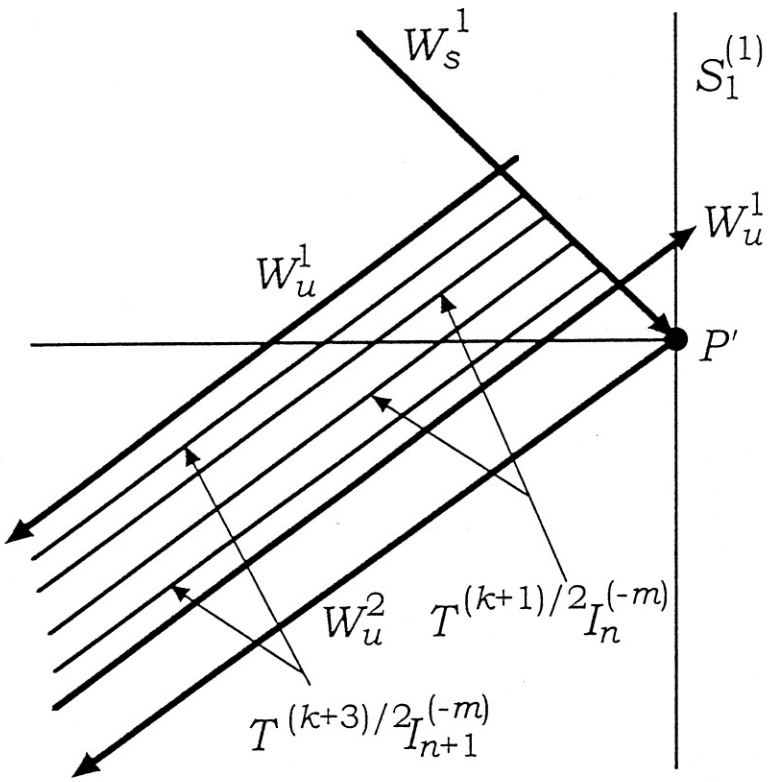

Fig. 4. Relation of $T^{(k+1)/2} I_n^{(-m)}$ and $T^{(k+3)/2} I_{n+1}^{(-m)}$.

Theorem 2. The following dynamical ordering for p/q–SNBPs in $K_n^{(-m)}$ and $L_n^{(-m)}$ holds where $0 \leq p \leq 2m+1$ for $K_n^{(-m)}$ and $0 \leq p \leq 2m$ for $L_n^{(-m)}$.

$K_0^{(-m)}, L_0^{(-m)}$:	$p/2$	$\rightarrow$	$p/3$	$\rightarrow$	$p/4$	$\rightarrow$	$p/5$	$\rightarrow$
	$\downarrow$		$\downarrow$		$\downarrow$		$\downarrow$	
$K_1^{(-m)}, L_1^{(-m)}$:	$p/4$	$\rightarrow$	$p/5$	$\rightarrow$	$p/6$	$\rightarrow$	$p/7$	$\rightarrow$
	$\downarrow$		$\downarrow$		$\downarrow$		$\downarrow$	
$K_2^{(-m)}, L_2^{(-m)}$:	$p/6$	$\rightarrow$	$p/7$	$\rightarrow$	$p/8$	$\rightarrow$	$p/9$	$\rightarrow$
	$\downarrow$		$\downarrow$		$\downarrow$		$\downarrow$	

Proof. Equations (44) and (45) determine the conditions for p. We prove the cases for SNBPs in $K_n^{(-m)}$. The proof for $L_n^{(-m)}$ is similar.
(1) Proof of $p/k \in K_n^{(-m)} \rightarrow p/(k+1) \in K_n^{(-m)}$ $(k \geq 2n+2)$.
(1-1) Both p and k are odd.

The assumption $p/k \in K_n^{(-m)}$ implies $T^{(k-1)/2}K_n^{(-m)} \cap S_{2-}^{-(m-(p-1)/2)} \neq \emptyset$. The intersection points are mapped to the left of $S_{4-}^{-(m-(p-1)/2)}$. This implies $T^{(k+1)/2}K_n^{(-m)} \cap S_{4-}^{-(m-(p-1)/2)} \neq \emptyset$.
(1-2) p is odd and k is even.

The assumption implies $T^{k/2}K_n^{(-m)} \cap S_{4-}^{-(m-(p-1)/2)} \neq \emptyset$. $T^{k/2}K_n^{(-m)} \cap S_{2-}^{-(m-(p-1)/2)} \neq \emptyset$ follows from the disposition of $S_{2-}^{-(m-(p-1)/2)}$ and $S_{4-}^{-(m-(p-1)/2)}$.
(1-3) p is even and k is odd.

The proof is similar to (1-1), and thus is omitted.
(1-4) Both p and k are even.

The proof is similar to (1-2), and thus is omitted.

(2) Proof of $p/k \in K_n^{(-m)} \rightarrow p/(k+2) \in K_{n+1}^{(-m)}$ $(k \geq 2n+2)$.
(2-1) Both p and k are odd.

The assumption $p/k \in K_n^{(-m)}$ implies $T^{(k-1)/2}K_n^{(-m)} \cap S_{2-}^{-(m-(p-1)/2)} \neq \emptyset$ and $T^{(k+1)/2}K_{n+1}^{(-m)} \dashv T^{(k-1)/2}K_n^{(-m)}$. This implies $T^{(k+1)/2}K_{n+1}^{(-m)} \cap S_{2-}^{-(m-(p-1)/2)} \neq \emptyset$.

For the other cases, the proofs are similar to (2-1), and thus are omitted. Q.E.D.

4.3 Accumulation of critical values

We now describe the behavior of critical values $a_c(1/(2i+j) \in I_i^{(0)})$ and $a_c(1/(2i+j) \in K_i^{(0)})$ as functions of i and j. We express the numerical results in a three–dimensional plot(see Figs. 5(a) and (b)). The maximum is $a_c(1/3 \in I_1^{(0)})$ in Fig. 5(a) and $a_c(1/2 \in K_0^{(0)})$ in Fig. 5(b). For a fixed i, the critical values decrease as j increases. The accumulation value is $a_c(I_i^{(0)})$ (resp., $a_c(K_i^{(0)})$).

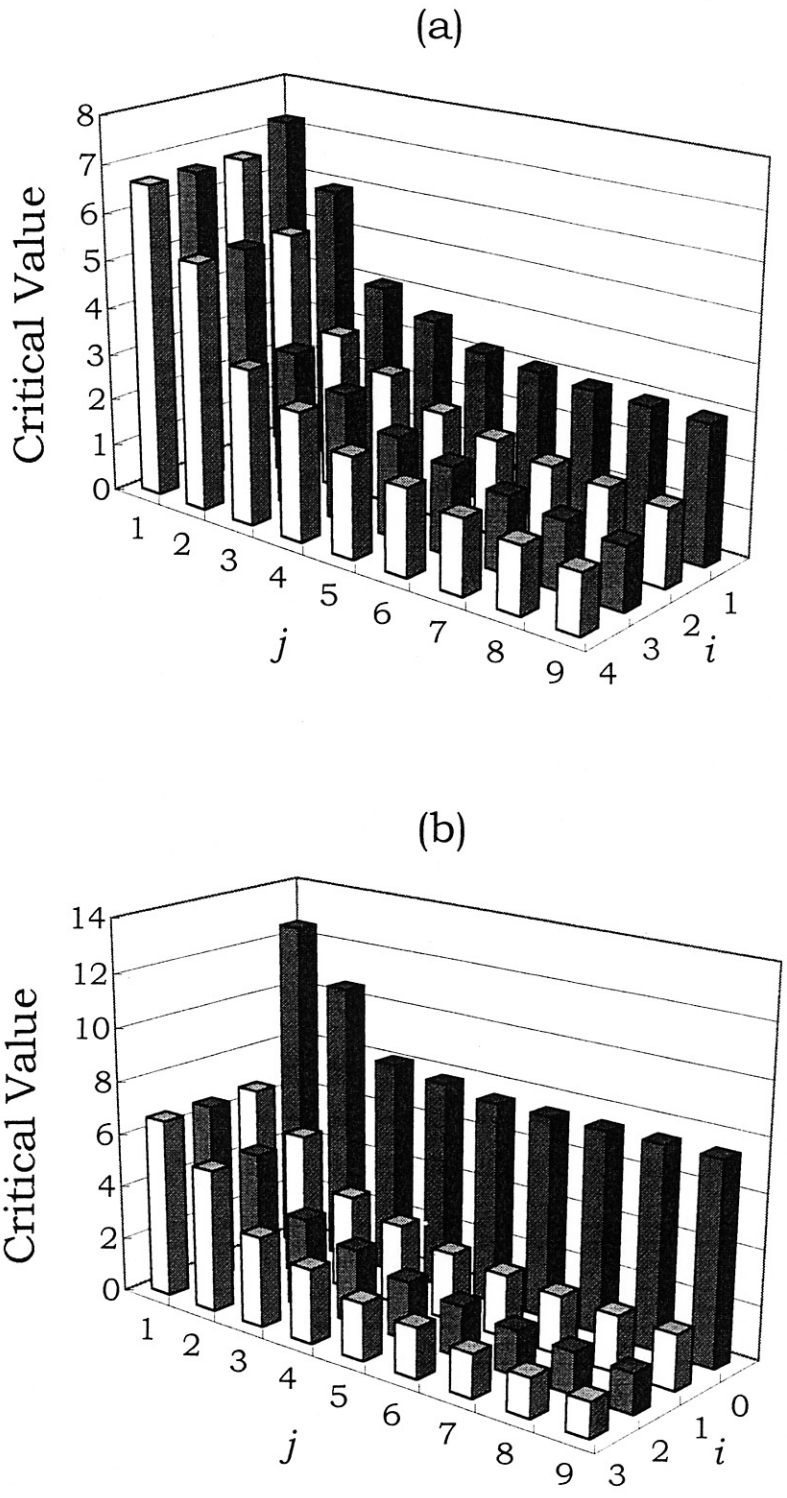

Fig. 5. Three–dimensional plot of (a) $a_c(1/(2i+j) \in I_i^{(0)})$ and (b) $a_c(1/(2i+j) \in K_i^{(0)})$

In the limit $i \gg 1$, the behavior of $a_c(I_i^{(0)})$ and $a_c(K_i^{(0)})$ displayed in Fig. 6 is modeled by

$$a_c(I_i^{(0)}),\ a_c(K_i^{(0)}) \ \propto \ \frac{1}{i^{\alpha}} \quad \text{with} \quad \alpha \simeq 0.93 \tag{48}$$

Here we discuss the meaning of taking the limit $i \to \infty$ for every j. We shall define two critical values. Let $a_c(n; S_{2,4-}^{(0)})$ be a critical value at which $T^n\gamma_u$ touches $S_{2,4-}^{(0)}$ for the first time. Repeating the same discussions in Properties 3.6-3.8, we have

$$\lim_{i\to\infty} a_c(1/(2i+j) \in I_j^{(0)}) \ = \ a_c(j; S_{2-}^{(0)})(j = 2n, n \geq 1), \tag{49}$$

$$\lim_{i\to\infty} a_c(1/(2i+j) \in I_j^{(0)}) \ = \ a_c(j; S_{4-}^{(0)})(j = 2n-1, n \geq 1), \tag{50}$$

$$\lim_{j\to\infty} a_c(j; S_{2,4-}^{(0)}) \ = \ 0. \tag{51}$$

The accumulation of $a_c(j; S_{2,4-}^{(0)})$ in the limit $j \to \infty$ is shown in Fig. 7 and is modeled by

$$a_c(j; S_{2,4-}^{(0)}) \propto \frac{1}{j^{\delta}} \quad \text{with} \quad \delta \simeq 0.87. \tag{52}$$

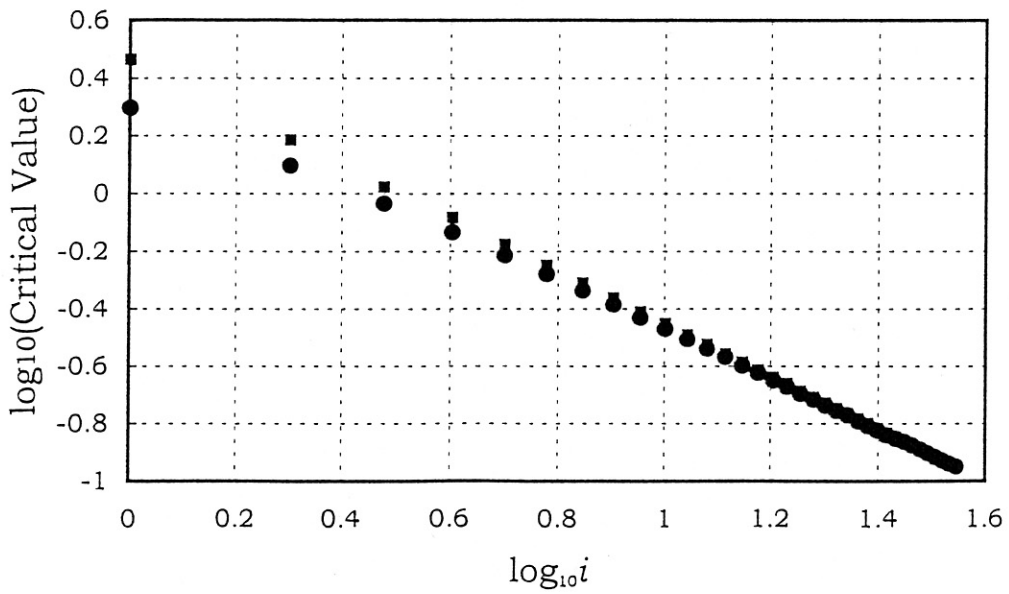

Fig. 6. Plot of $a_c(I_i^{(0)})$(square) and $a_c(K_i^{(0)})$(circle) as a function of i.

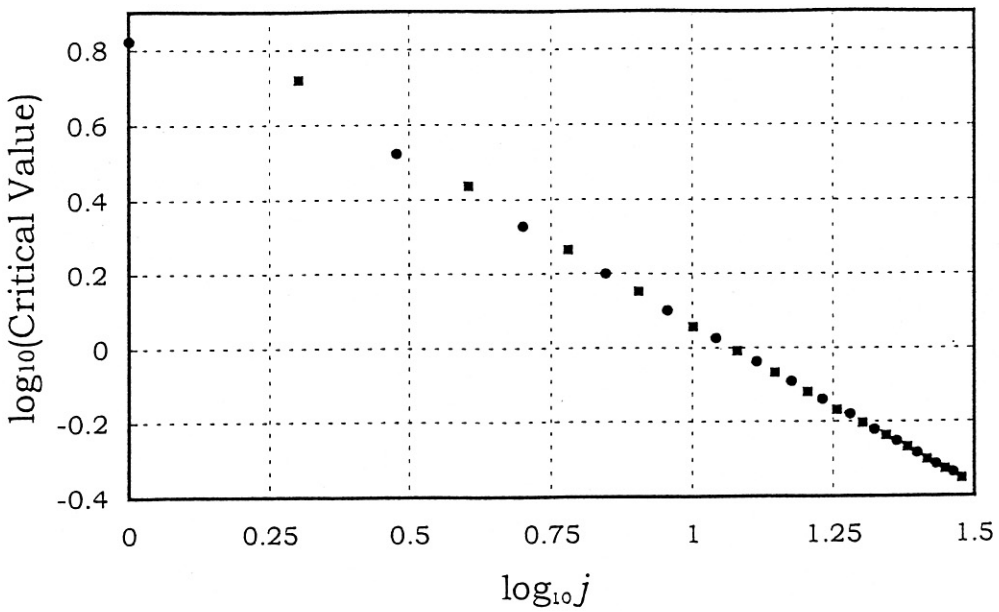

Fig. 7. Accumulation of critical values $a_c(j; S^{(0)}_{2^-})$ (square) and $a_c(j; S^{(0)}_{4^-})$ (circle).

5 Braid

We express the reason why we construct the braid of SNBO. If there exists a particular periodic orbit in the system and its braid is *pseudo-Anosov* (pA) type, the lower bound of topological entropy is positive and thus there exists chaos in this system. The concept of pA is an extension of Anosov property showing the hyperbolicity of system.[28)]

Let us introduce notation. $\mathrm{DO}^p_{R(-m)}$ $(R = I, J, K, \text{or } L)$ represents the dynamical order itself realized in R where p shows the numerator of rotation number. $\mathrm{DO}^p_{R(-m)}(i, j)$ $(R = I, J, K, \text{or } L)$ is the (i, j) element of $\mathrm{DO}^p_{R(-m)}$ where $i \geq 1$ and $j \geq 1$ for $I^{(-m)}$ and $J^{(-m)}$, and $i \geq 0$ and $j \geq 1$ for $K^{(-m)}$ and $L^{(-m)}$.

5.1 Braid for SNBOs in $\mathrm{DO}^1_{I^{(0)}}$

For an $1/(2i+j)$–SNBO with $j = 2k+1, k \geq 0, i \geq 1$, we divide its orbital points $\{p_0, p_1, \ldots, p_{2i+2k}\}$ of one period into four groups $\mathcal{A}, \mathcal{B}, \mathcal{C}$ and $\mathcal{D}$ as

$$\mathcal{A} = \{p_0, \cdots, p_{i-1}\}, \quad \mathcal{B} = \{p_i, \cdots, p_{i+k}\},$$
$$\mathcal{C} = \{p_{i+k+1}, \cdots, p_{i+2k+1}\}, \quad \text{and} \quad \mathcal{D} = \{p_{i+2k+2}, \cdots, p_{2i+2k}\}$$

where p_0 is always taken in $I_i^{(0)}$, $\mathcal{A}\backslash\{p_0\}$ and $\mathcal{C}$ are located between $S_1^{(0)}$ and $S_2^{(0)}$, and $\mathcal{B}$ and $\mathcal{D}$ between $S_2^{(0)}$ and $S_1^{(1)}$. We have $\mathcal{A}\backslash\{p_0\} = G\mathcal{D}$ and $\mathcal{B} = G\mathcal{C}$ by reversibility.

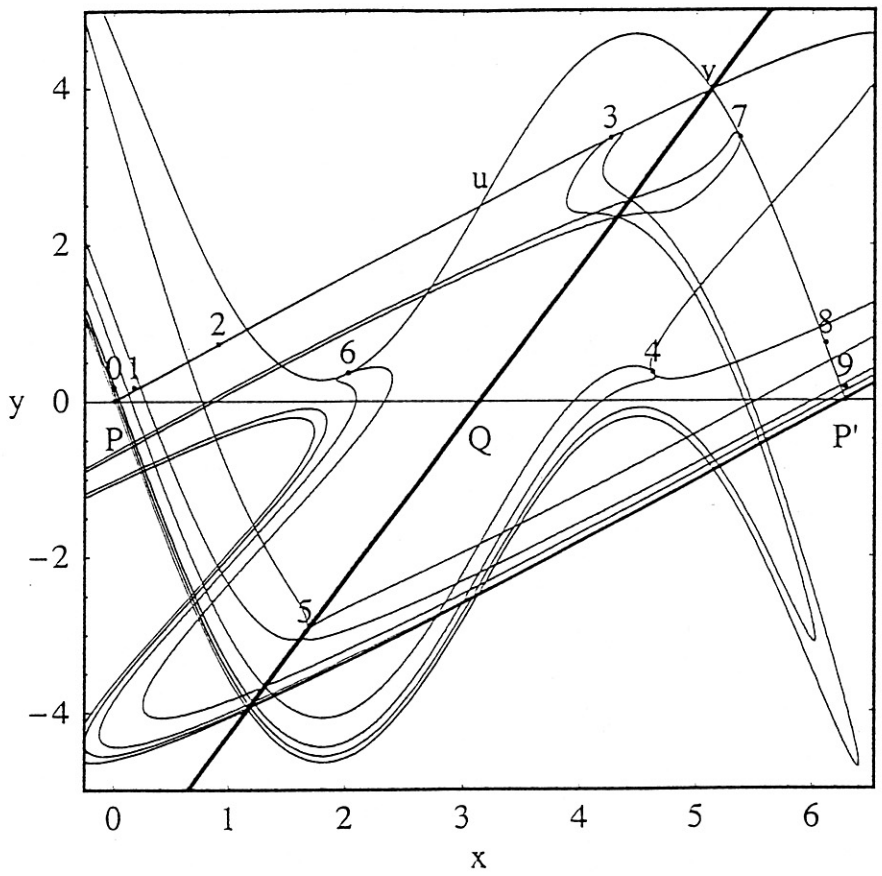

Fig. 8. The orbit of an 1/9–SNBP in $I_3^{(0)}$ where an integer k stands for p_k. The stable and unstable manifolds are also displayed.

Figure 8 displays the orbit of an 1/9–SNBP in $I_3^{(0)}$ where $\mathcal{A} = \{p_0, p_1, p_2\}$, $\mathcal{B} = \{p_3, p_4\}$, $\mathcal{C} = \{p_5, p_6\}$ and $\mathcal{D} = \{p_7, p_8\}$. The schematic version is illustrated in Fig. 9(a). The group $\mathcal{A}$ is located to the left of W_u^1 and $\mathcal{C}$ is to the right. Due to the reversibility with respect to $S_2^{(0)}$, $\mathcal{B}$ is located to the right of W_s^1 and $\mathcal{D}$ is to the left.

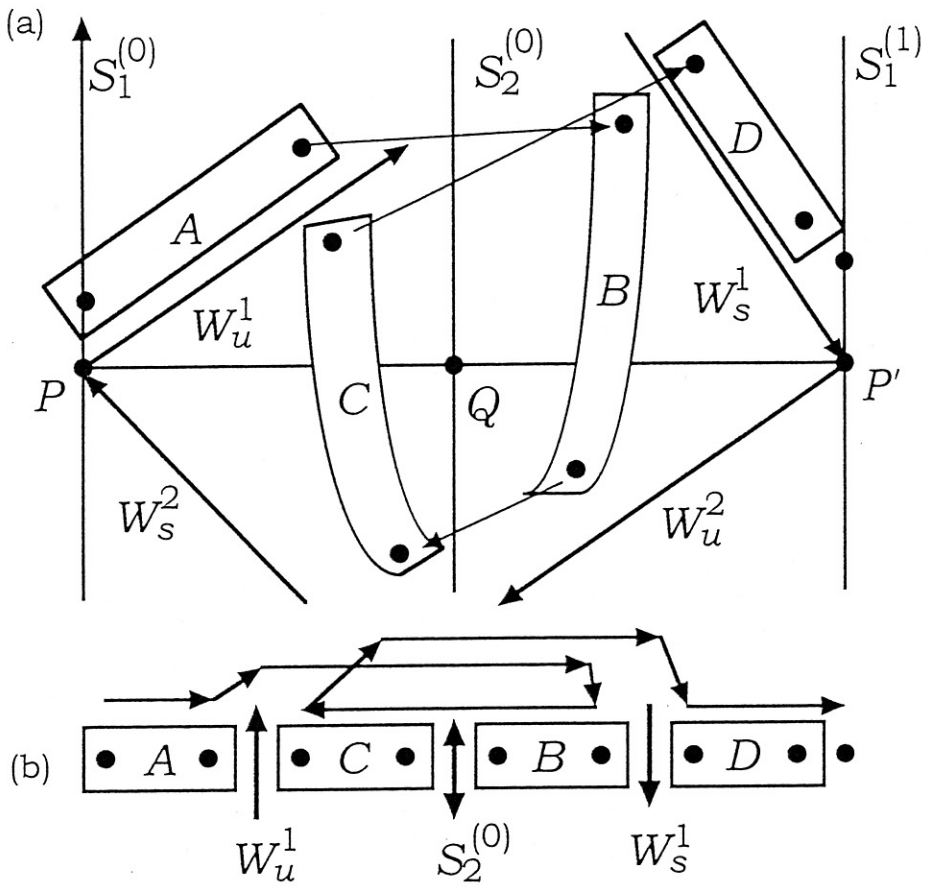

Fig. 9. (a) Configuration of four groups $\mathcal{A}, \mathcal{B}, \mathcal{C}$ and $\mathcal{D}$, and (b) reconstruction of these groups into the fundamental orbital order.

For the behavior of the orbital points, we observe the following properties. These are justified next paragraph.

[P1] There is one turing point in $\mathcal{B}$ and $\mathcal{C}$.

[P2] For the points in $\mathcal{A}$ and $\mathcal{D}$, the following relations hold.

$$\pi_1(p_m) < \pi_1(p_{m'}) \tag{53}$$

where $0 \leq m < m' \leq i-1$ in $\mathcal{A}$ and $i+2k+2 \leq m < m' \leq 2i+2k)$ in $\mathcal{D}$.

[P3] For the points in $\mathcal{A}$ and $\mathcal{C}$, the following relations hold if the corresponding points exist at all.

$$\pi_1(p_{i-1}) < \pi_1(p_{i+2k+1}), \tag{54}$$

$$\pi_1(p_{i-2}) < \pi_1(p_{i+2k}), \tag{55}$$

$$\cdots.$$

[P4] For the points in $\mathcal{B}$ and $\mathcal{D}$, the following relations hold if the corresponding points exist at all.

$$\begin{aligned} \pi_1(p_i) &< \pi_1(p_{i+2k+2}), & (56)\\ \pi_1(p_{i+1}) &< \pi_1(p_{i+2k+3}), & (57)\\ &\cdots. \end{aligned}$$

[P5] The x coordinate of any point in $\mathcal{B}$ is larger than those of points in $\mathcal{C}$.

Here [P1] means that one turning–back point is located in $\mathcal{B}$ and one turning–forward point in $\mathcal{C}$. [P2] means that the orbital points in $\mathcal{A}$ and $\mathcal{D}$ are well–ordered. In fact, the turning back does not occur since the value of y–coordinate of orbital points is positive. Equation (56) in [P4] is true since $p_i \in V$ and $p_{i+2k+2} \in TU$, and TU is located to the right of V. The other inequalities reflect the fact that p_{i+2k+2} in TU is mapped to the right of Tv and p_i in V is mapped to the left of Tv, and so on. Note that $p_{2i+2k+1} \in T^iU$ is located in $S^{(1)}_{1+}$ and $p_{i+k+1} \in T^{k+1}V$ is located in $S^{(0)}_{4-}$. Operating G to the equations of [P4], we have [P3]. [P5] is derived from the reversibility with respect to G.

Taking into account [P1] through [P5], we place the four groups of points in a line as

$$O_o(i,j) = (\mathcal{A} \uparrow \mathcal{C} \updownarrow \mathcal{B} \downarrow \mathcal{D}). \tag{58}$$

A schematic illustration is given in Fig. 9(b). We call the expression an *orbital order* of $\mathrm{DO}^1_{I(0)}(i,j)$. The suffix o stands for 'odd', i.e., Eq. (58) is for odd periodic orbits. Three symbols $\uparrow, \updownarrow$ and $\downarrow$ in the orbital order represent W^1_u, S^0_2, and W^1_s, respectively. These symbols stress that four groups are separated by three objects. Later, these will be frequently omitted. If in particular p_k and p_{i+k+1} are the two turning points and there are no other turning points, then we call the order the *fundamental orbital order* (FOO). The role of the FOO in constructing braids will be seen in what follows.

Let us consider $\mathrm{DO}^1_{I(0)}(3,3)$. Its FOO(see Fig. 10(a)) is

$$O_o(3,3) = (012654378). \tag{59}$$

There are two additional orbital orders which satisfy [P1-5] and which can be realized by actual orbits(Fig. 10(b) and (c)):

$$O'_o(3,3) = (012563478), \tag{60}$$

$$O''_o(3,3) = (015263748). \tag{61}$$

We can not exchange 1 and 5 due to [P3], and 4 and 8 due to [P4]. The orbital order directly determined by the orbit displayed in Fig. 8 is $O'_o(3,3)$.

We describe now the construction of a braid of an $1/q$–SNBO using the information on the orbital order. A braid is constructed in two steps. The first step is a construction of $(q-1)$ strings from 0 to 1, 1 to 2, ..., $(q-2)$ to $(q-1)$, and the second step is that of the final string from $(q-1)$ to 0.

Step [1]. A string corresponding to the forward motion goes behind a string corresponding to the backward motion when they cross.
Step [2]. The string from $(q-1)$ to 0 goes behind all other strings when they cross.
The first rule expresses the twist property and the second one the rigid rotation with $\nu = 1/q$ revolving round cylinder.

Braid $\beta(3,3)$ constructed from $O_o(3,3)$ is shown in Fig. 10(a). Its expression in terms of generators is

$$\beta(3,3) = \sigma_4^{-1}\sigma_5^{-1}\sigma_6^{-1}\sigma_3^{-1}\sigma_4^{-1}\sigma_5^{-1}\zeta_9, \tag{62}$$

where $\zeta_9 = \sigma_8 \cdots \sigma_1$. Braid $\beta'(3,3)$ constructed from $O'_o(3,3)$ and braid $\beta''(3,3)$ from $O''_o(3,3)$(Figs. 10(b) and (c)) are expressed in terms of generators as

$$\beta'(3,3) = \sigma_6^{-1}\sigma_5^{-1}\sigma_6^{-1}\sigma_3^{-1}\sigma_4^{-1}\sigma_3^{-1}\zeta_9, \tag{63}$$

$$\beta''(3,3) = \sigma_7^{-1}\sigma_6^{-1}\sigma_5^{-1}\sigma_4^{-1}\sigma_3^{-1}\sigma_2^{-1}\zeta_9. \tag{64}$$

These braids are equivalent to $\beta(3,3)$ via the Markov move as

$$\beta'(3,3) = \sigma_4\sigma_6^{-1}\beta(3,3)\sigma_4^{-1}\sigma_6, \tag{65}$$

$$\beta''(3,3) = \sigma_3\sigma_7^{-1}\beta'(3,3)\sigma_3^{-1}\sigma_7. \tag{66}$$

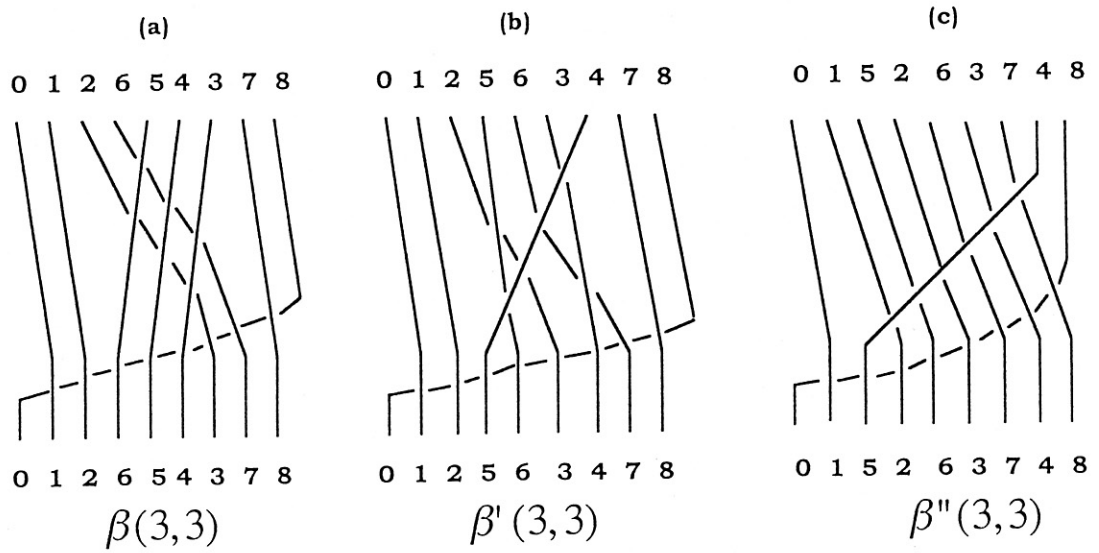

Fig. 10. (a) Braid constructed from $O_o(3,3)$, (b) that from $O'_o(3,3)$ and (c) that from $O''_o(3,3)$ where an integer k stands for p_k.

To obtain $\beta''(3,3)$, we exchange two strings 4 and 7 in $\beta'(3,3)$. The string from 7 to 8 gets ahead of the string from 4 to 5 in the upper side. As a result, new intersection point appears. We add σ_7^{-1} in the left side of $\beta'(3,3)$. In the bottom, the string from 3 to 4 and the string from 6 to 7 do not intersect each other. In order to untwist them,

we add σ_7 in the right of $\beta'(3,3)$. Due to symmetry, we add σ_3 and σ_3^{-1} and thus have $\beta''(3,3)$. It turns out that the exchange of points in the orbital order does not change the braid type if it does not violate [P1-5]. The construction of the FOO is simple compared with that of other orbital orders. This is the reason why we use the FOO to construct the braid.

Let us see what happens if we accomplish inhibited exchanges of two strings 3 and 7 and of strings 2 and 6 in Fig. 10(a). These exchanges do not satisfy [P3] and [P4]. We have an orbital order (016254738) and have a braid $\sigma_7^{-1}\beta(3,3)\sigma_3^{-1}$. Since the number of intersection points of braid is different from that of $\beta(3,3)$, the new braid is not equivalent to $\beta(3,3)$.

Let us next consider periodic orbits of even period. We divide the orbital points (one period) of an $1/(2i+j)$–SNBO ($j=2k, k\geq 1$) into $\{p_{i+k}\}$ and four sets $\mathcal{A},\mathcal{B},\mathcal{C}$, and $\mathcal{D}$ as

$$\mathcal{A}=\{p_0,\cdots,p_{i-1}\},\quad \mathcal{B}=\{p_i,\cdots,p_{i+k-1}\},$$
$$\mathcal{C}=\{p_{i+k+1},\cdots,p_{i+2k}\},\quad \text{and}\quad \mathcal{D}=\{p_{i+2k+1},\cdots,p_{2i+2k-1}\}.$$

and arrange them in a line as

$$O_e(i,j)=(\mathcal{A}\uparrow\mathcal{C}(\widehat{i+k})\mathcal{B}\downarrow\mathcal{D}). \tag{67}$$

where $(\widehat{i+k})$ stands for $p_{i+k}\in S_{2-}^{(0)}$. The symbols have the same meaning as before. $(\widehat{i+k})$ plays the role of $\updownarrow$. The FOO is defined as the orbital order in which turning points are p_i and p_{i+k}.

Now the expressions of braids for $O_o(2,3)=(0154326)$ and $O_e(2,4)=(01654\hat{3}27)$ are determined.

$$\begin{aligned}\beta(2,3) &= \sigma_3^{-1}\sigma_4^{-1}\sigma_5^{-1}\sigma_2^{-1}\sigma_3^{-1}\sigma_4^{-1}\zeta_7,\\ &= \sigma_1^{-1}\sigma_2^{-1}\sigma_3^{-1}\sigma_3^{-1}\sigma_2^{-1}\sigma_1^{-1}\zeta_7,\end{aligned} \tag{68}$$

$$\begin{aligned}\beta(2,4) &= \sigma_3^{-1}\sigma_4^{-1}\sigma_5^{-1}\sigma_6^{-1}\sigma_2^{-1}\sigma_3^{-1}\sigma_4^{-1}\sigma_5^{-1}\zeta_8,\\ &= \sigma_1^{-1}\sigma_2^{-1}\sigma_3^{-1}\sigma_4^{-1}\sigma_4^{-1}\sigma_3^{-1}\sigma_2^{-1}\sigma_1^{-1}\zeta_8,\end{aligned} \tag{69}$$

where Reidemeister and Markov moves[5),24)] are operated to derive the second equation in Eqs. (68) and (69). As a result, the expression of braid for $O_o(i,j)$ or $O_e(i,j)$ is derived.

$$\beta(i,j)=\zeta_{j+1}^{-1}\rho_{j+1}^{-1}\zeta_{2i+j} \tag{70}$$

where $\rho_k=\sigma_1\cdots\sigma_{k-1}$ and $\zeta_k=\sigma_{k-1}\cdots\sigma_1$.

Here let us compare $\beta(i,j)$ and braids investigated by Boyland.[8)] Consider two annuli and $(2i+j)$ strings connecting them. The braid $\zeta_{j+1}^{-1}\rho_{j+1}^{-1}$ means that the first string passes behind the second through $(j+1)$-th strings, and then passes in front of these strings. This twisting is caused by the non–Birkhoffness of the orbit. The braid ζ_{2i+j} represents a rigid rotation of a $1/(2i+j)$–Birkhoff orbit. According to this geometrical interpretation, the braid $\beta(i,1)$ corresponds to the braid constructed by Boyland.

5.2 Braid for SNBOs in $\mathrm{DO}^1_{K^{(0)}}$

5.2.1 Braid for SNBOs in $\mathrm{DO}^1_{K^{(0)}}$ with $i \geq 1$

Figure 11 displays SNBOs starting in $S^{(0)}_{3+}$. The points of one period of an orbit are grouped into four sets $\mathcal{A}, \mathcal{B}, \mathcal{C}$ and $\mathcal{D}$. For even period $q = 2i + j + 1$ ($j = 2k - 1, k \geq 1$), we define the orbital order.

$$\begin{aligned} O_e(i,j) &= (\mathcal{A} \uparrow \mathcal{C} \updownarrow \mathcal{B} \downarrow \mathcal{D}), \qquad (71) \\ \mathcal{A} = \{p_0, \cdots, p_{i-1}\}, &\quad \mathcal{B} = \{p_i, \cdots, p_{i+k-1}\}, \\ \mathcal{C} = \{p_{i+k}, \cdots, p_{i+2k-1}\}, &\quad \text{and} \quad \mathcal{D} = \{p_{i+2k}, \cdots, p_{2i+2k-1}\}. \end{aligned}$$

The FOO is such that p_i and p_{i+2k-1} are the turning points. For odd period $q = 2i + j + 1$ ($j = 2k, k \geq 1$), we define the orbital order.

$$\begin{aligned} O_o(i,j) &= (\mathcal{A} \uparrow \mathcal{C}(\widehat{i+k})\mathcal{B} \downarrow \mathcal{D}), \qquad (72) \\ \mathcal{A} = \{p_0, \cdots, p_{i-1}\}, &\quad \mathcal{B} = \{p_i, \cdots, p_{i+k-1}\}, \\ \mathcal{C} = \{p_{i+k+1}, \cdots, p_{i+2k}\}, &\quad \text{and} \quad \mathcal{D} = \{p_{i+2k+1}, \cdots, p_{2i+2k}\}. \end{aligned}$$

The FOO is such that p_i and p_{i+2k} are the turning points. Note that $\mathcal{A} = G\mathcal{D}$ and $\mathcal{C} = G\mathcal{B}$ hold in both $O_e(i,j)$ and $O_o(i,j)$.

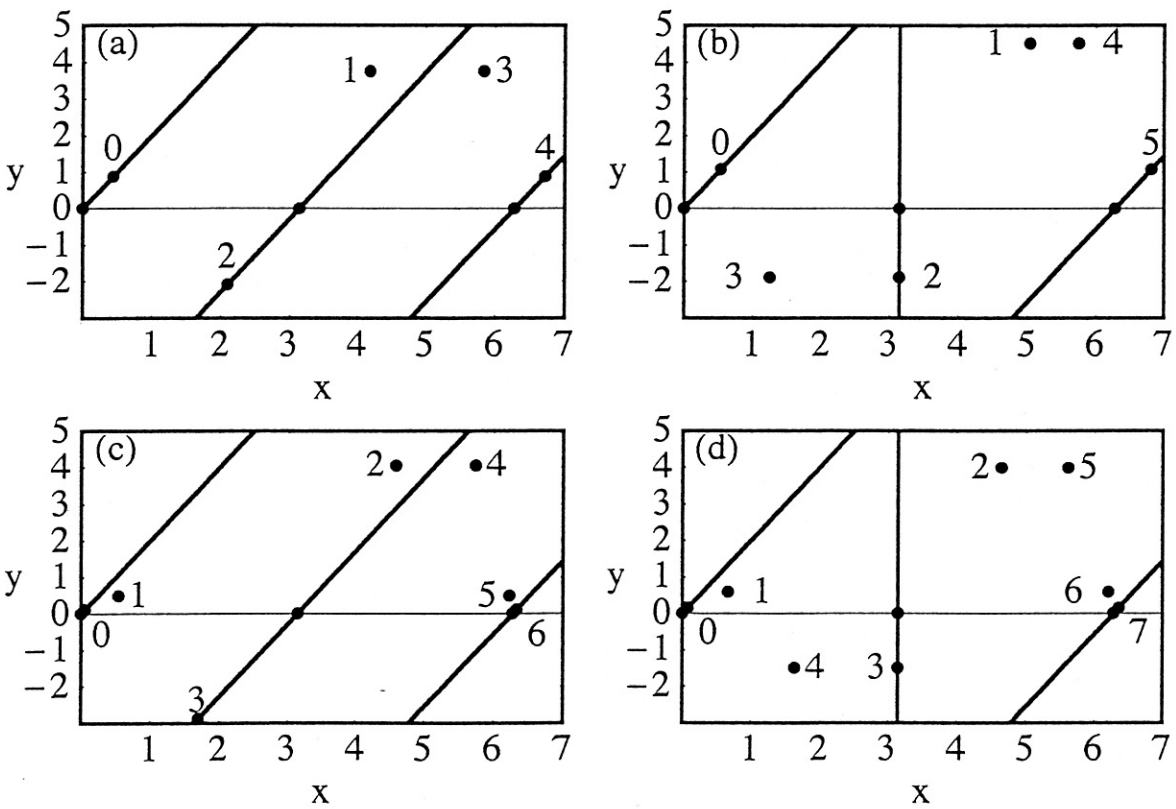

Fig. 11. (a) $1/4 \in K^{(0)}_1$, (b) $1/5 \in K^{(0)}_1$, (c) $1/6 \in K^{(0)}_2$ and (d) $1/7 \in K^{(0)}_2$.

Using the same rules as in §5.1, the braid $\beta(i,j)$ for $\mathrm{DO}^1_{K^{(0)}}(i,j)$ is derived.

$$\beta(i,j) = \zeta_{j+1}^{-1}\rho_{j+1}^{-1}\zeta_{2i+j+1}. \tag{73}$$

5.2.2 Braid for SNBOs in $\mathrm{DO}^1_{K^{(0)}}$ with $i = 0$

In Fig. 12, two orbits with $\nu = 1/2$ and $1/3$ are displayed. For both orbits, the turning back of the orbit occurs at p_0 (symbol 0 in the figure).

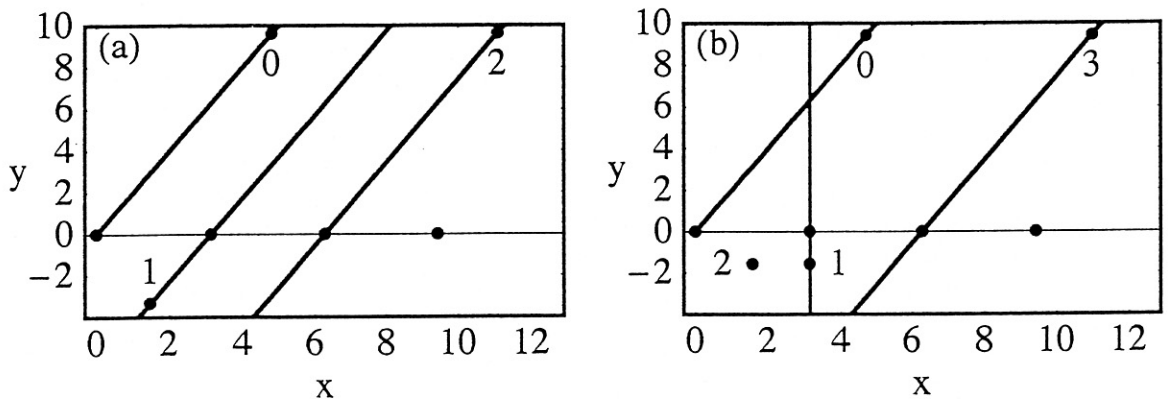

Fig. 12. (a) $1/2 \in K_0^{(0)}$ and (b) $1/3 \in K_0^{(0)}$.

In order to have a braid of pA from an 1/2–SNBO ($\mathrm{DO}_{K^{(0)}}(0,1)$), we need at least one more string. To accomplish this, we use the information in the vicinity of the period–2 orbit. We first deform cylinder to annulus. Next we shrink the inner circle of annulus to a point (termed as c). The point c stands for the fixed point at infinity. A string from c to c is the additional string. We construct the braid of three strings connecting two annuli. Let a string from p_0 to p_1 be A, a string from p_1 to p_0 be B and a string from c to c be C. Two strings A and B revolve round c. This gives how to intersect two strings (A and C, B and C). If A and B intersect each other, we draw the string of the forward motion behind the string of the backward motion. This intersection corresponds to the twist property. As a result, we have the expression of braid.

$$\beta(0,1) = \sigma_1\sigma_2^{-1}\sigma_1^{-1}\sigma_2\sigma_2 = \sigma_1^2\sigma_2^{-1}. \tag{74}$$

The braid $\beta(0,1)$ expresses the tangled structure of the braid of the period–2 orbit and that of c.

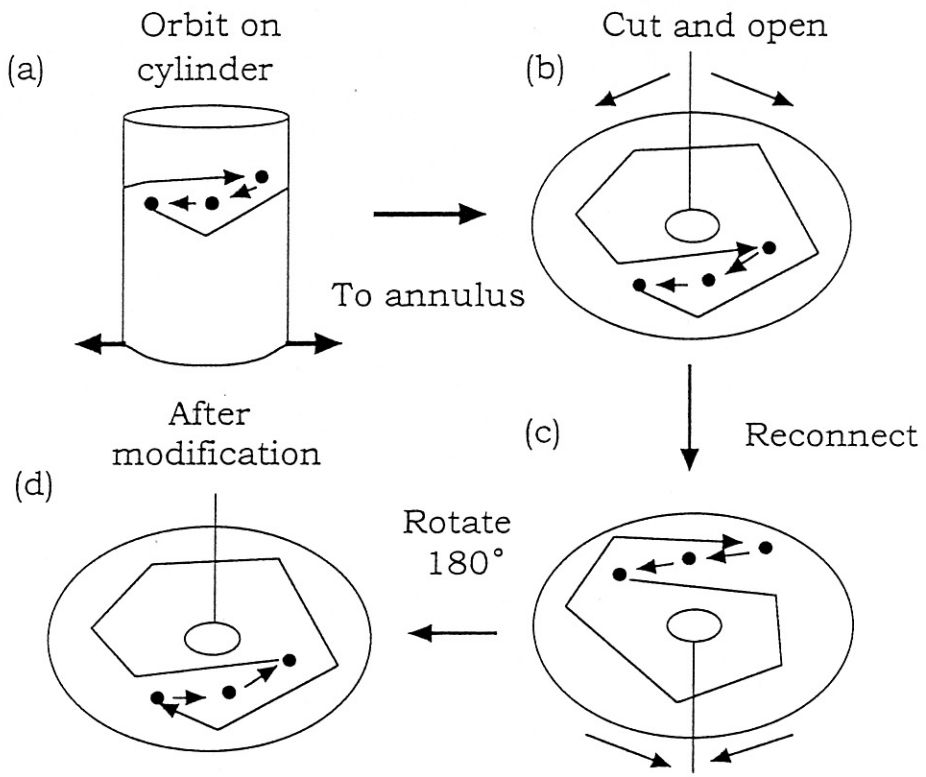

Fig. 13. Deformation of cylinder to annulus ((a) $\rightarrow$ (b)). Cutting and recombination of annulus ((b) $\rightarrow$ (c)). After rotating (c) by 180°, we have (d)

Next we construct the braid for an 1/3–SNBO. The orbital order is $O_o = (\uparrow 2\hat{1}0 \downarrow)$, and this gives a braid $\sigma_1^{-1}\sigma_2^{-1}$. But this braid is not pA. We apply the transformation illustrated in Fig. 13. The first step is the deformation of cylinder to annulus. We cut open annulus and glue both borders at the opposite side so that the inner and outer circles exchange their role. Thus we have new orbit in the modified annulus and have the expression of braid.

$$\begin{aligned} \beta(0,2) &= \sigma_2^{-1}\sigma_1^{-1}\sigma_1^{-1}\sigma_2^{-1}\sigma_2^{-1}\sigma_1^{-1}, \\ &= (\sigma_2^{-1}\sigma_1^{-1})^3\sigma_1\sigma_2^{-1}. \end{aligned} \tag{75}$$

Equation (75) implies that $\beta(0,2)$ is pA.

The orbital orders for the elements with $j(\geq 2)$ of $q = j + 1$ are derived.

$$O_o(0,j) = (\uparrow \mathcal{B}\hat{k}\mathcal{A} \downarrow), \tag{76}$$

where $\mathcal{A} = (p_0, \cdots, p_{k-1})$, $\mathcal{B} = (p_{k+1}, \cdots, p_{2k})$ $(j = 2k, k \geq 1)$ and p_0 and p_{2k} are the turning points, and

$$O_e(0,j) = (\uparrow \mathcal{B} \updownarrow \mathcal{A} \downarrow), \tag{77}$$

where $\mathcal{A} = (p_0, \cdots, p_k)$, $\mathcal{B} = (p_{k+1}, \cdots, p_{2k+1})$ $(j = 2k+1, k \geq 1)$ and p_0 and p_{2k+1} are the turning points. In both expressions, $\mathcal{B} = G\mathcal{A}$ holds.

These determine the braids $\sigma_1^{-1}\cdots\sigma_q^{-1}$. Unfortunately these are not pA. Therefore, we apply the transformation mentioned above and then have the braids of pA.

$$\beta(0,j) = \rho_{j+1}^{-2}\zeta_{j+1}^{-1} \ (j \geq 2). \tag{78}$$

6 Topological entropy

We have derived braids of SNBOs in §5. In this section, we use these to estimate the lower bound of the topological entropy of a system which possesses an SNBO with braid β. The lower bound $h(\beta)$ of the entropy can be estimated by the maximum absolute eigenvalue ($\lambda_{max} = \mathrm{Max}(|\lambda_i|)$) of the reduced Burau matrix representation $M_\beta(t)$.[25),26)]

$$h(\beta) = \ln \lambda_{max}. \tag{79}$$

The reduced Burau matrix representation $M_\beta(t)$ has a parameter t defined by $t = \exp(i\theta)$ $(0 \leq \theta < 2\pi)$. In order to calculate $h(\beta)$, we need the value of $\mathrm{Max}(|\lambda_i|)$ as a function of t or θ. For the braid of the third order, λ_{max} is obtained at $t = -1$.[23)] We need numerical calculations for the braids of arbitrary orders. In Appendix, we give a sample program written by MATHEMATICA[27)] to construct the reduced Burau matrix representation and to calculate its eigenvalues. Figure 14 displays the numerical results of $\mathrm{Max}(|\lambda_i|)$ as a function of θ.

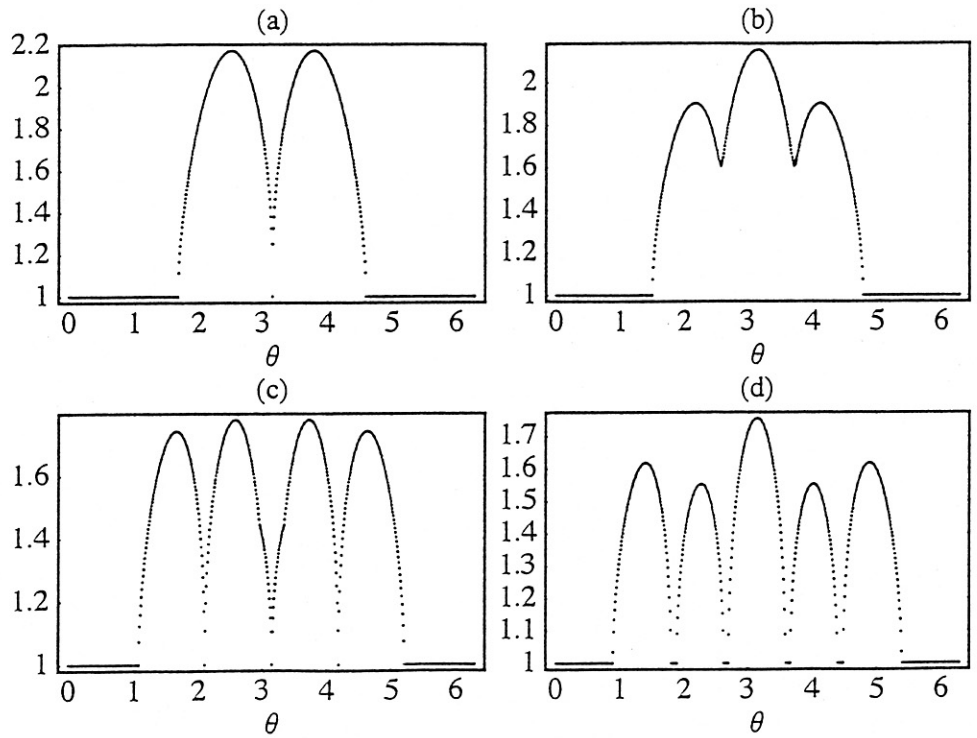

Fig. 14. The θ dependence of $\mathrm{Max}(|\lambda_i|)$. (a) $1/4 \in I_1^{(0)}$,(b) $1/5 \in I_1^{(0)}$,(c) $1/6 \in I_2^{(0)}$ and (d) $1/7 \in I_2^{(0)}$.

6.1 Topological entropy estimated by using SNBO in $\mathrm{DO}^1_{I(0)}$

We observe the following property for braids of odd orders through numerical calculations. Proof is in order. The property is generally not true for braids of even orders. Then we only calculate $h(\beta)$ for SNBOs with odd periods.

Observation. λ_{max} is determined by the maximum absolute value of the real root(> 1) of eigenfunction at $t = -1$.

We derive the eigenfunction of the reduced Burau matrix for braid $\beta(1,j) = \zeta_{j+1}^{-1}\rho_{j+1}^{-1}\zeta_{j+2}$ in $\mathrm{DO}^1_{I(0)}(1,j)$ where j is assumed to be an odd integer satisfying $j \geq 1$. For example, Eq. (80) gives the reduced Burau matrix with $t = -1$ for $\beta(1,3) = \sigma_3^{-1}\sigma_2^{-1}\sigma_1^{-1}\sigma_4$ of $1/5 \in I_1^{(0)}$, and Eq. (81) is its eigenfunction.

$$M_{\beta(1,3)}(-1) = \begin{pmatrix} 1 & -1 & 0 & 0 \\ 1 & 0 & -1 & 0 \\ 1 & 0 & 1 & -1 \\ 0 & 0 & -1 & 1 \end{pmatrix}, \tag{80}$$

$$\lambda^4 - 3\lambda^3 + 3\lambda^2 - 3\lambda + 1 = 0. \tag{81}$$

The eigenfunction for any j is obtained in Eq.(82).

$$\lambda^{j+1} + 3\sum_{k=1}^{j}(-\lambda)^k + 1 = \frac{(\lambda-2)(\lambda^{j+1}-2)-3}{\lambda+1} = 0. \tag{82}$$

It is easy to see that the value of λ_{max} accumulates at 2 as $j \to \infty$. Equation (82) corresponds to the expression derived by Boyland.[8)]

In order to estimate λ_{max} for (i,j) element, we shall derive the eigenfunction for the cases with $j > i$.

$$\sum_{k=0}^{2i-2}(2k+1)(-\lambda)^k + (4i-1)\sum_{k=2i-1}^{j}(-\lambda)^k + \sum_{k=j+1}^{2i+j-1}(4i+2j-2k-1)(-\lambda)^k = 0. \tag{83}$$

Our main purpose is to estimate the topological entropy in the limit $i,j \to \infty$. Here we consider the limit $j \to \infty$. We keep the most divergent terms in Eq. (83), and let these be zero.

$$\lambda^{2i-1}(\lambda - 1) = 2. \tag{84}$$

Next we consider the cases with $i > j$ and thus have

$$\sum_{k=0}^{j-1}(2k+1)(-\lambda)^k + (2j+1)\sum_{k=j}^{2i-1}(-\lambda)^k + \sum_{k=2i}^{2i+j-1}(4i+2j-2k-1)(-\lambda)^k = 0. \tag{85}$$

We also have

$$(-\lambda)^j(1-\lambda) = 2. \tag{86}$$

For the cases with $j = 2i - 1$, the accumulation values $\hat{h}$ of topological entropy $h(\beta(i,j))$ at the i–th row and the j–th column are same. Let us consider the limit $i, j \to \infty$. Put $\lambda = 1 + \epsilon(\epsilon > 0)$. In the case with $\epsilon \ll 1$, we have the relation $\hat{h} \approx \epsilon$. Equations (84) is rewritten in the form:

$$k \ln(1 + \epsilon) = \ln(2/\epsilon) \tag{87}$$

where $k = 2i - 1$. In the limit $k \to \infty$, we have the topological entropy $\hat{h}$:

$$\hat{h} = \frac{\ln(2k)}{k} + O\left(\frac{\ln(\ln(2k))}{k}\right). \tag{88}$$

Numerical results of Eq. (87) are shown in Fig. 15. For large values of k, these results are in agreement with Eq. (88).

Equation (88) gives that the topological entropy is zero in the integrable limit and also means that the system with $a > 0$ is pA. Combining Eqs. (48) and (88), we have the topological entropy $\hat{h}$ as a function of a in the limit $a \to 0$.

$$\hat{h} \propto \frac{\ln(1/a)}{(1/a)^{1/\alpha}}. \tag{89}$$

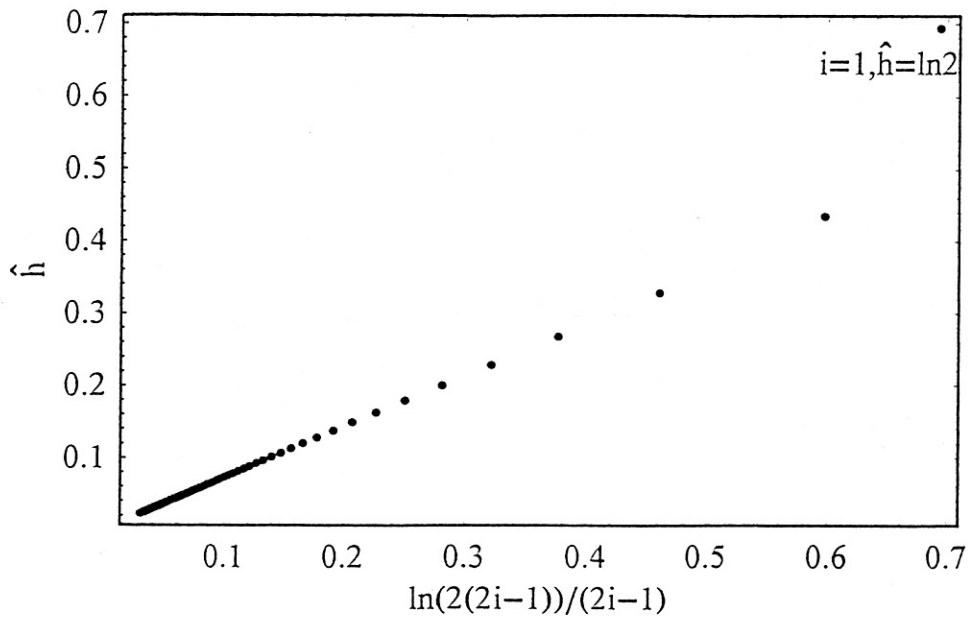

Fig. 15. Accumulation of topological entropy $\hat{h}$.

6.2 Topological entropy estimated by using SNBO in $\mathrm{DO}^1_{K^{(0)}}$

The topological entropy for $\mathrm{DO}^1_{K^{(0)}}(0,1)$ has been already estimated in Ref. 22).

$$h(\beta(0,1)) = 2 + \sqrt{3}. \tag{90}$$

We derive the eigenfunction of $\mathrm{DO}^1_{K^{(0)}}(0,j)$ for even j since Observation of §6.1 is true in these cases.

$$(\lambda+3)\lambda^{j+1} = 1+3\lambda. \tag{91}$$

In the limit $j \to \infty$, we have $|\lambda| \to 3$.

Next we study the topological entropy for $\mathrm{DO}^1_{K^{(0)}}(i,j)(i \geq 1)$. In these cases, Observation of §6.1 is not true (see Fig. 16). Thus we calculate the topological entropy numerically. The accumulation value of the topological entropy of the limit $j \to \infty$ at $i = 1$ is $\ln 1.63$, and that of the limit $i \to \infty$ at $j = 1$ is $\ln 2$. The topological entropies $\hat{h}_i(i \geq 1, j \to \infty)$ and $\hat{h}_j(j \geq 1, i \to \infty)$ are displayed in Fig. 17, and accumulate to zero in the limit $i, j \to \infty$ showing the integrable limit.

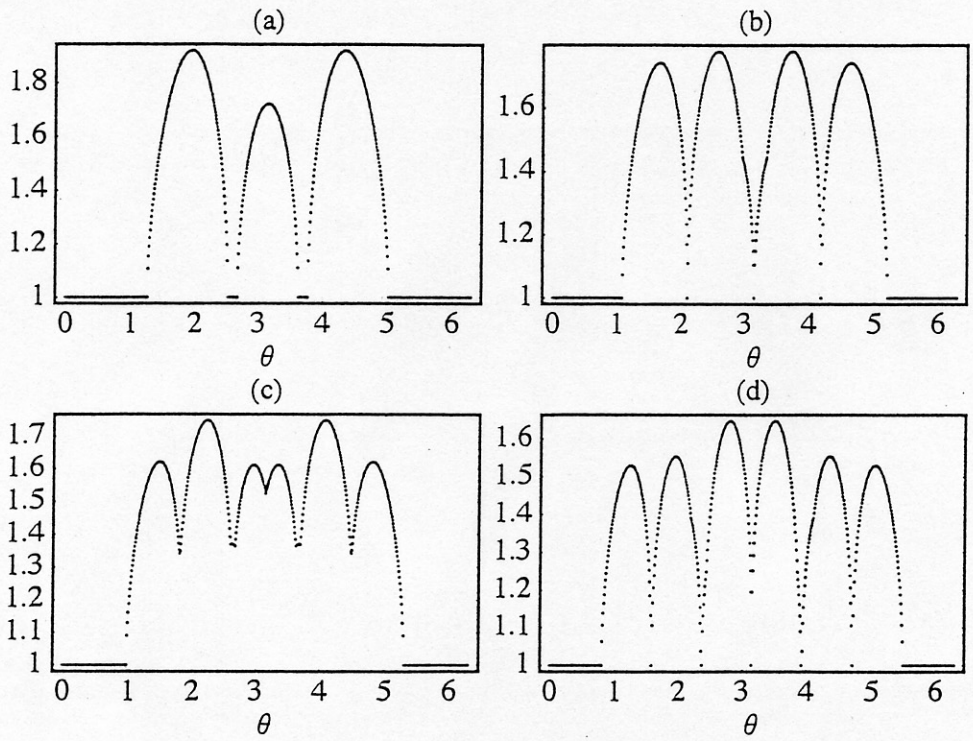

Fig. 16. The θ–dependence of $\mathrm{Max}(|\lambda_i|)$. (a) $1/5 \in K_1^{(0)}$,(b) $1/6 \in K_1^{(0)}$,(c) $1/7 \in K_2^{(0)}$ and (d) $1/8 \in K_2^{(0)}$.

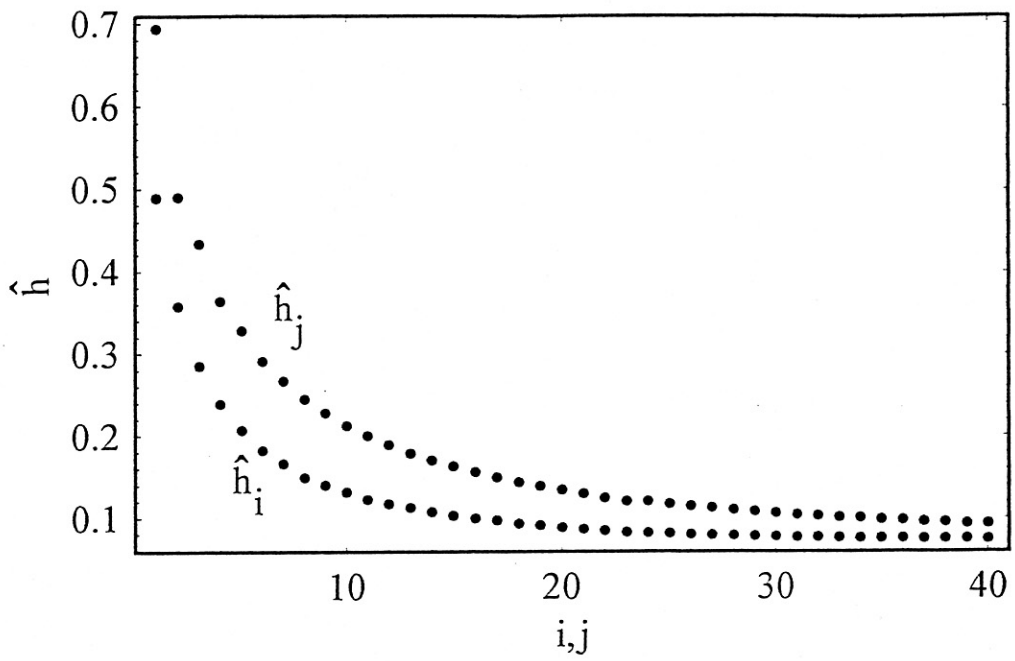

Fig. 17. Accumulation of topological entropy.

7 Remarks

We refer to several points to be pursued.

[1] Forcing relation between different dynamical orderings, for example, $\mathrm{DO}^{p}_{I(0)}$ and $\mathrm{DO}^{p'}_{K(0)}$.

To establish the relation, $p/2$– or $p/3$–SNBOs plays an important role.

[2] Dynamical ordering for the SNBOs with $2n$ ($n \geq 2$) turning points and the estimation of topological entropies for these orbits.

[3] Appearance order of NBOs not having points in symmetry axes.

We have a hypothesis for their appearance, i.e., all NBOs not having points in symmetry axes are bifurcated from mother SNBOs.

[4] Dynamical ordering for SNBOs of Type II.

This will be useful to investigate the breakup of KAM curves.

[5] Appearance of NBOs in the systems not having the left-right symmetry.

We believe that two theorems proved in §4 are true if the symmetry breaking perturbation is weak.

[6] Forcing relation between the braids obtained in §5.

Can we derive the dynamical ordering of SNBOs by using it? This is a reverse approach.

[7] Theoretical explanation of the power law decay of critical values obtained as Eqs. (48) and (52).

Acknowledgements

The authors express their thanks to Drs. T. Matsuoka and E. Kin for discussions.

References

1) K. Tanikawa and Y. Yamaguchi, *Chaos* **12** (2002), 33.
2) Y. Yamaguchi and K. Tanikawa, Prog. Theor. Phys. **106** (2001), 1097.
3) A. Sharkovskii, Ukr. Mat. Z. **16** (1964), 61.
4) L. Alsedà, J. Llibre and M. Misiurewicz, *Combinatorial Dynamics and Entropy in Dimension One* (World Scientific, 1993).
5) T. Matsuoka, in *Dynamical System* **1** (World Scientific, 1986), p. 58; Contemp. Math. **152** (1993), 229. See also Bussei Kenkyu(Kyoto) **67** (1996), 1.
6) P. Boyland, Contemp. Math. **81** (1988), 119.
7) S. Baldwin, Ergod. Th. & Dynam. Sys. **11** (1991), 249.
8) P. Boyland, Topology and its Appl. **58** (1994), 223.
9) M. Handel, Ergod. Th. & Dynam. Sys. **17** (1997), 593.
10) J. Los,*I.H.E.S.* (1997), 5.
11) P. Boyland and G. R. Hall, Topology **26** (1987), 21.
12) I. Leage and R. S. Mackay, Phys. Lett. A **118** (1986), 274.
13) G. D. Birkhoff, Acta. Math. **43** (1920), 44.
14) K. Tanikawa and Y. Yamaguchi, J. Math. Phys. **28** (1987), 921: **30** (1989), 608.
15) G. R. Hall, Ergod. Theor. & Dynam. Sys. **4** (1984), 585.
16) R. de Vogelaere, in *Contribution to the Theory of Nonlinear Oscillations* Vol.IV (Princeton University Press, 1957).
17) P. Le Calvez, *Dynamical Properties of Diffeomorphisms of the Annulus and of the Torus* (AMS, 2000).
18) V. F. Lazutkin, I. G. Schachmannski and M. B. Tabanov, Physica D, **40** (1989),235.
19) S. Wiggins, *Chaotic Transport in Dynamical Systems* (Springer–Verlag, 1991).
20) Y. Yamaguchi and K. Tanikawa, Prog. Theor. Phys. **103** (2000), 1127.
21) J. Palis and W. de Melo, *Geometric Theory of Dynamical Systems* (Springer, 1982).
22) Y. Yamaguchi and K. Tanikawa, Prog. Theor. Phys. **106** (2001), 691.
23) Y. Yamaguchi and K. Tanikawa, Prog. Theor. Phys. **104** (2000), 943.
24) S. Moran, *The Mathematical Theory of Knots and Braids* (North–Holland, 1983).
25) D. Fried, in *Geometric Dynamics.* ed. J. Palis Jr. Lecture Notes in Mathematics **1007** (Springer–Verlag, 1983). p. 261.
26) B. Kolev, C. R. Acad, Sci. Paris, **309**, Ser. I (1989), 835.
27) S. Wolfram, *THE MATHEMATICA BOOK*, Fourth Edition (Cambridge University Press, 1999).
28) A. J. Casson and S. A. Bleiber, *Automorphisms of Surface after Nielsen and Thurston* (Cambridge University Press, 1988).

Appendix

A MATHEMATICA (Trademark of Wolfram Research) program which constructs the reduced Burau matrix representation and calculates its eigenvalues as a function of θ is shown below.

Explanatory note.
[1] In the first block, input two values of **n** (≥ 4) and **ma** where **n** is an order of braid and **ma** is a number of division of θ.
[2] The second block is a preparation of generators.
[3] In the third block, input a braid by using **s[k]** and **is[k]** where **s[k]** is a generator σ_k and **is[k]** a generator σ_k^{-1}.
[4] In the fourth block, the eigenvalues are calculated and $\mathrm{Max}|\lambda_i|$ is displayed as a function of θ. Final output is λ_{max}.

A sample program determines the eigenvalues of a braid $\sigma_1\sigma_2^{-1}\sigma_3^{-1}$.

Sample program

```
(* 1st Block *)
(* Input an order of Braid *)
n = 4;
(* Input a number of division *)
ma = 360;

(* 2nd Block *)
(* Construction of generators s[1] - s[n - 1] and is[1] - is[n - 1] *)
Clear[t];
nn = n - 1; m = 1; v = {0};
Do[v = Append[v, 0], {k, 1, nn - 1}];
Do[d[i] = ReplacePart[v, 1, i], {i, 1, nn}];
d[m] = ReplacePart[d[m], -t, m];
d[m] = ReplacePart[d[m], 1, m + 1];
s[m] = Table[d[k], {k, 1, nn}];
m = 1; v = {0};
Do[v = Append[v, 0], {k, 1, nn - 1}];
Do[d[i] = ReplacePart[v, 1, i], {i, 1, nn}];
d[m] = ReplacePart[d[m], -1/t, m];
d[m] = ReplacePart[d[m], 1/t, m + 1];
is[m] = Table[d[k], {k, 1, nn}];
Do[v = {0};
    Do[v = Append[v, 0], {k, 1, nn - 1}];
    Do[d[i] = ReplacePart[v, 1, i], {i, 1, nn}];
    d[m] = ReplacePart[d[m], t, m - 1];
    d[m] = ReplacePart[d[m], -t, m];
```

```
    d[m] = ReplacePart[d[m], 1, m + 1];
    s[m] = Table[d[k], {k, 1, nn}], {m, 2, nn - 1}];
Do[v = {0};
    Do[v = Append[v, 0], {k, 1, nn - 1}];
    Do[d[i] = ReplacePart[v, 1, i], {i, 1, nn}];
    d[m] = ReplacePart[d[m], 1, m - 1];
    d[m] = ReplacePart[d[m], -1/t, m];
    d[m] = ReplacePart[d[m], 1/t, m + 1];
    is[m] = Table[d[k], {k, 1, nn}], {m, 2, nn - 1}];
m = nn; v = {0};
Do[v = Append[v, 0], {k, 1, nn - 1}];
Do[d[i] = ReplacePart[v, 1, i], {i, 1, nn}];
d[m] = ReplacePart[d[m], t, m - 1];
d[m] = ReplacePart[d[m], -t, m];
s[m] = Table[d[k], {k, 1, nn}];
m = nn; v = {0};
Do[v = Append[v, 0], {k, 1, nn - 1}];
Do[d[i] = ReplacePart[v, 1, i], {i, 1, nn}];
d[m] = ReplacePart[d[m], 1, m - 1];
d[m] = ReplacePart[d[m], -1/t, m];
is[m] = Table[d[k], {k, 1, nn}];
(* end *)

(* 3rd Block *)
(* Input a braidtype  *)
b = s[1].is[2].is[3];

(* 4th Block *)
  (* Calculation of Eigenvalues *)
Do[
    theta = 2Pi/ma*k;
    t = Cos[theta] + I*Sin[theta];
    gg = Eigenvalues[N[b]];
    Do[e[i] = Abs[Part[gg, i]], {i, 1, nn}];
    y[k] = Max[Table[e[k], {k, 1, nn}]];
    x[k] = N[theta], {k, 0, ma}];
  (* Output *)
g1 = Table[{x[k], y[k]}, {k, 0, ma}];
ListPlot[g1, PlotStyle -> {RGBColor[1, 0, 0]}];
gg = Table[y[k], {k, 0, ma}];
Max[gg]
```

If the eigenfunction of the reduced Burau matrix with $t = -1$ is needed, delete the fourth block and add the following statements.

```
(* Eigenfunction: f(x) = 0. Output is f(x). *)
t = -1;
Det[b - x*IdentityMatrix[n - 1]]
```